A physically-based model for strain-induced crystallization in natural rubber. Part II: Derivation of the mechanical model

Alice Gros, Erwan Verron, Bertrand Huneau

A physically-based model for strain-induced crystallization in natural rubber. Part II: derivation of the ~~thermo-~~mechanical model

Alice Gros, Erwan Verron, Bertrand Huneau

ECN - GeM

Institut de Recherche en Génie Civil et Mécanique (GeM), UMR CNRS 6183, École Centrale de Nantes, BP 92101, Nantes Cedex 3, France

Abstract

Despite the numerous experimental investigations performed over the past century and more intensively in the last fifteen years, strain-induced crystallization in natural rubber still remains hardly understood in its precise mechanisms, limiting most of constitutive equations to phenomenological approaches. The present Part II of our work aims to develop a physically-motivated constitutive equation which qualitatively reproduces phenomena observed during deformation. Firstly, the amorphous network is assumed to deform in an equal-force manner, resulting in a representative chain encompassing the inhomogeneity of cross-linking into the chain-length distribution. Then, as proposed in Part I of this work, crystallization and melting conditions are considered, based on classical thermodynamics and on the entangled nature of the polymer network. Finally, a semi-crystallized chain is defined, accounting for both the inhomogeneity of the amorphous phase and the heterogeneity due to the presence of a crystalline phase. This chain is included in a modified full-network model, initially dedicated to amorphous networks. This work leads to a ~~thermo-~~mechanical constitutive equation which qualitatively reproduces the mechanical response of natural rubber.

Keywords: constitutive equations; thermodynamics; phase transitions; chain-length distribution; entanglements.

1. Introduction

Thanks to important progress in X-ray measurement techniques, the intensive experimental investigations of these last fifteen years on strain-induced crystallization of natural rubber improved our knowledge of this complex phenomenon (Tosaka, 2007; Huneau, 2011; Toki, 2014; Albouy and Sotta, 2015;

Email address: erwan.verron@ec-nantes.fr (Erwan Verron)

Candau et al., 2014, 2015a,b,c, 2016). In spite of that, these results do not allow yet to fully understand the nature of the involved mechanisms, and consequently, most of the corresponding constitutive equations are phenomenological (Kroon, 2010; Mistry and Govindjee, 2014; Guilié et al., 2015; Nateghi et al., 2018; Rastak and Linder, 2018; Khiêm and Itskov, 2018). These models aim to reproduce the change of crystalline degree in uniaxial tension cycle and the corresponding mechanical response, schematized in Figure 1: both the increase in

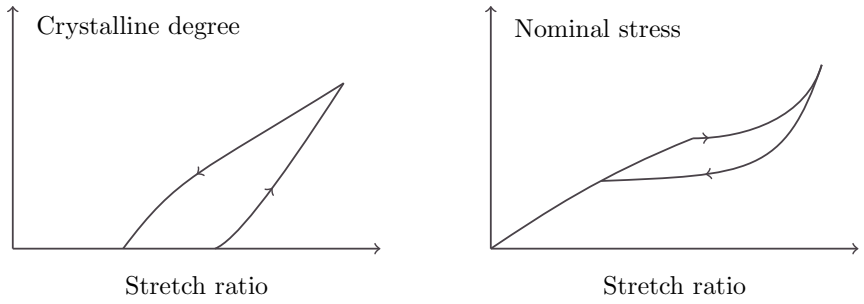

Figure 1: Usual shape of the experimental (a) crystalline degree and (b) nominal stress vs. stretch ratio curves.

crystalline fraction during sample stretching and its melting during the unload process (Fig. 1(a)) apparently influence the mechanical response (Fig. 1(b)). Development of models strikes into the problem of defining a realistic and physical threshold of crystallization, and of finding an explanation to the hysteresis observed between loading and unloading paths. In fact, the complexity of the phenomena is an obstacle to a clear vision of the problem, inviting to limit oneself to phenomenological descriptions that generally do not take into account detailed thermodynamical aspects, which yet govern phase transitions.

As described in Part I of this work (Gros et al., 2018), the model developed by Laghmach et al. (2015) stands out from phenomenological models by tackling the thermodynamic aspects of nucleation, crystallization and melting. Thermodynamical analysis of experimental results of Candau et al. (2014, 2015b) also represents an attractive approach giving an insight on thresholds of phase transition based on network inhomogeneity. However, these two models are not included in a robust ~~thermo-~~mechanical tridimensional framework. The very first model proposed by Flory (1947) for semi-crystallized chain (described in 2.1.1) constitutes an important link between the thermodynamic (or physical) approach and the derivation of a one-dimensional mechanical model: it considers a freely-jointed chain (succession of freely rotating Kuhn segments) in which crystallization is represented as an alignment in the loading direction of consecutive segments that become elastically ineffective. Mechanical tridimensional constitutive equations have been developed for unfilled natural rubber by Kroon (2010), Mistry and Govindjee (2014), Guilié et al. (2015), Nateghi et al. (2018), Rastak and Linder (2018), and Khiêm and Itskov (2018). Their framework is systematic: *(i)* modeling the unidirectional behavior of a crys-

tallizing chain using Flory's representation, *(ii)* choosing an evolution law for crystallization, *(iii)* establishing how to include it in the mechanical framework, and then *(iv)* creating a tridimensional model using a mean-field transition. This one-dimensional to tridimensional transition has been subject to developments in fully amorphous cases, from the 3-, 4- or 8-chain models (using the unidirectional behavior in some representative directions of the space) to a full-network model considering all the material directions (James and Guth, 1943; Wang and Guth, 1952; Flory and Rehner, 1943; Treloar, 1975, 1954; Treloar and Riding, 1979; Wu and van der Giessen, 1993; Arruda and Boyce, 1993; Miehe et al., 2004). However, in these works, crystallization is merely modeled by an equation governing the evolution of macroscopic crystalline degree, which avoids tackling the threshold of crystallization, the reasons of a progressive evolution and the influence on mechanical behavior. In fact, Kroon (2010) uses an Arrhenius law of nucleation kinetics, and viscosity effects are added in the one-dimensional chain response to produce the hysteretic mechanical response. Mistry and Govindjee (2014) refuse the use of viscosity from experimental arguments, and propose to model crystallization evolution with a function similar to a chemical potential: this law is used as a threshold and global driving function of crystallization, tuned by two parameters controlling how favored crystallization is and how fast crystalline degree increases. Such function is also used by Guilié et al. (2015), who add a strengthening effect of crystallization similar to a plasticity law. Nateghi et al. (2018) use a similar approach but considering a dissipation potential for melting process. Rastak and Linder (2018) choose a simpler law linking crystallization force and rate of crystallization. Khiêm and Itskov (2018) choose to focus on crystallite growth and calorimetric effects but the fundamental approach for considering the thermodynamics of crystallization and melting is not very different from the others. Although these models effectively reproduce the two experimental characteristic curves of Fig. 1, their parameters govern the crystallization evolution law and hence they elude the difficulties inherent to the modeling of crystallization physics. Another recent publication by Plagge and Klüppel (2018) takes a more physical approach, close to ours, to derive a simple but efficient model. It will be further commented in Remark 1 in Section 2.

Given this context, the main objective of a relevant new model of strain-induced crystallization consists in including a physical description of crystallization, but keeping at the same time the tools of mechanical modeling of amorphous networks which are now well grounded. The present paper proposes a model based on the same four-step scheme as the other mechanical models, improved by more advanced thermodynamical features of phase transition as well as topological aspects of the network as introduced in Part I of this work (Gros et al., 2018). Facing the complexity of the problem and encouraged by the variety of existing experimental results, some important physical characteristics standing out from the experimental studies are first extracted, and then mechanical and thermodynamical frameworks taking into account these features are defined in order to derive constitutive equations. After an overview of the choices of important physical features of the network, the model is derived in

Section 2. A dedicated algorithm is proposed in Section 3, along with its results in Section 4 discussing the influence of the parameters. We also take advantage of the proposed approach to observe the evolutions of physical quantities with strain involving strain-induced crystallization.

2. Model derivation

The general framework of this model, devoted to unfilled crosslinked natural rubber undergoing static deformations, is the same as those described in the Introduction: deriving a one-dimensional model representative of the material behavior in one direction, and considering it in different directions in space to build a tridimensional constitutive equation. A material point is thus considered as a unit sphere with chains spreading in all directions in space, each of these chains being representative of the material behavior in the corresponding direction. The following key physical features of the network, highlighted from experimental investigations, are required: the *inhomogeneity* of the network, the *entangled* nature of the chains in the network creating topological constraints, the coexistence of amorphous and crystallized phases leading to semi-crystallized *heterogeneous* chains, and the existence of preferential chain *orientation* during the deformation of the network. These features appear in the four main steps of the derivation, which are summarized hereby and detailed thereafter in four respective sections.

1. *Representation of the chain-length inhomogeneity* (section 2.1.2)
   The inhomogeneity of the network is due to the randomness of crosslinking in natural rubber resulting in a distribution of chain-length, as experimentally investigated by Ikeda et al. (2008) and pointed out by Candau et al. (2014) as being strongly involved in strain-induced crystallization. Unfortunately, the chain length distribution (*a.k.a* molecular weight distribution) in the network is unknown, and is hence considered as an input parameter of the model. The network is thus seen as a set of homogenous subnetworks which we shall refer to as *populations*, each of them being comprised of chains having the same length, following an idea introduced by Candau et al. (2014, 2015b). The assumption of an equal-force deformation leads to a convenient way of describing the amorphous representative chain behavior, as proposed in (Verron and Gros, 2017).
2. *Crystallization and melting conditions in an entangled network* (section 2.1.3)
   Classical theories applied to homogenous networks are used, along with new topological conditions: crystallites cannot appear or grow freely because of chain entanglements in the network, as described in Part I (Gros et al., 2018). These topological constraints were also considered by Laghmach et al. (2015) and mentioned by Candau et al. (2014) to stop crystallites growth (which is assumed to be instantaneous considering the experimental results by Tosaka et al. (2012)). The importance of topological considerations is also emphasized by experimental results by Trabelsi

et al. (2003) where sizes of stabilized crystallites formed in a priorly deformed network are closely related to the dimensions of an available volume around an entanglement in the deformed network. The model input parameters are here the interface energies needed in thermodynamic equations, and a distribution of entanglements relating to each chain length a length between two entanglements.

3. *Definition of a semi-crystalline representative chain* (section 2.2)
   Crystallization and melting conditions are applied to each of the populations constituting the representative chain, which hence becomes semi-crystalline. Although the general idea of the semi-crystallized chain introduced by Flory (1947) and recalled in section 2.1.1 is kept, the way we model the crystallites requires to adapt it by taking into account entanglements. The states before and after crystallization must also be properly defined because of a change in chain-length distribution with crystallization. The general behavior of the semi-crystallized representative chain, specifically its stretch ratio, its force and its crystalline degree, are expressed and this constitutes the one-dimensional model.
4. *Integration in a tridimensional framework* (section 2.3)
   The transition to a tridimensional model is accomplished through an adaptation of the *full-network* model proposed in (Verron and Gros, 2017) whose theory accounts for the chain-length distribution of the network. It catches in particular the chain behavior for each direction, which is particularly important since crystallization is strongly dependent on chain orientation (Toki et al., 2004; Amnuaypornsri et al., 2012) and leads to a strong anisotropy. However, this full-network model did not include crystallization, which is thus properly introduced in the present paper in the equations in order to complete the ~~thermo-~~mechanical tridimensional model.

Remark 1. *As stated in the Introduction, the recent work by Plagge and Klüppel (2018) also considers a physically-based model based on similar ideas as introduced in our work. Major similarities and differences are detailed here. First of all, the main similarity is the idea of using a limitation of growth of crystallite by topological constraints as we introduced in Part I, although its treatment using entropic repelling potential to be included in the total entropy of the semi-crystallized chain is very different. Secondly, one major difference is that the one-dimensional model is based on entropic consideration (while ours focuses on stretch ratios and forces). Force is introduced when integrating the 1D to a tridimensional framework, which uses the most basic 3-chain model. A noteworthy novelty of our work is the consideration of chain-length distribution, which is our driving reason for crystallization to occur progressively and a way of capturing a better mechanical response. In spite of simplifying assumptions, the model of Plagge and Klüppel captures very well experimental features at both micro and macro scales such as crystallite size evolution and dependency of onset and offset of crystallization on temperature.*

2.1. Prerequisites

2.1.1. Flory's representation of a semi-crystallized chain

First of all, let us recall the basic representation of a semi-crystallized chain, introduced by Flory (1947). An amorphous chain is modeled as an ideal chain, characterized by its number of statistical Kuhn segments N (in the following, we refer to such chain as an N-chain). The relationship between its stretch ratio λ (ratio between deformed and initial length) and force f is defined as follows for non-gaussian chains:

$$f = \frac{k_B T}{b} \mathscr{L}^{-1}\left(\frac{\lambda}{\sqrt{N}}\right), \tag{1}$$

where b is the length of a Kuhn segment, k_B stands for the Boltzmann constant, T is the absolute temperature, and $\mathscr{L}$ is the Langevin function defined by:

$$\mathscr{L} : \left| \begin{array}{l} \mathbb{R} \to]-1\,;\,1[\\ x \mapsto \begin{cases} 0 & \text{if} \quad x = 0\,, \\ \coth(x) - (1/x) & \text{otherwise.} \end{cases} \end{array} \right. \tag{2}$$

Flory's representation consists in considering that when crystallization takes place while the chain deforms, some successive segments representing the crystalline phase get aligned in the loading direction (it is assumed that their entropy vanishes), as represented in Figure 2. This model explains in particular

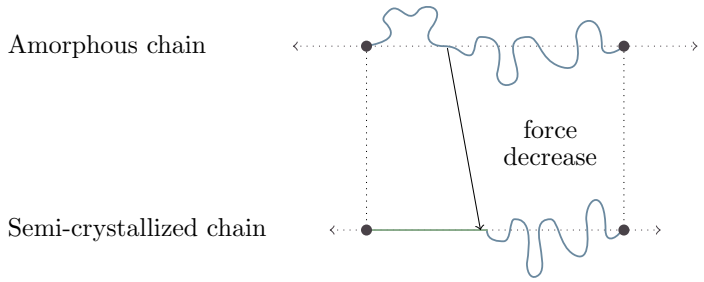

Figure 2: Flory's representation: a portion of the chain aligns with loading (horizontal) direction when crystallization occurs (left part of the chain), leading to a force decrease in the remaining amorphous part.

the force decrease experimentally observed when crystallization occurs. In the present work, the aims consist of enriching the amorphous part, defining when and how segments crystallize, in order to get a semi-crystallized chain and finally use this one-dimensional model to derive a tridimensional constitutive equation.

2.1.2. Representative amorphous inhomogeneous chain and full-network model

In order to achieve the enrichment of the amorphous part and the transition to a tridimensional constitutive equation, the framework of a full-network model accounting for a network having a chain-length distribution introduced in Verron

and Gros (2017) is used: the constitutive equation is derived by integrating the one-dimensional response of a polymer chain over the unit sphere, and each one-dimensional chain accounts for the distribution of chain length. The general result used in the present work is that given the sole knowledge of a chain-length distribution, a tridimensional model accounting for it in each direction in space can be derived. Equations strictly necessary to our model derivation are recalled here with adapted notations.

The inhomogeneous (one-dimensional) chain is made of populations (groups of chains having the same length in the network) indexed by a generic subscript i (in $I = \{1, 2, 3, ...N_{\max}\}$), and characterized by the number N_i of segments of its chains and the proportion (in number of chains) ϕ_i in the network. Assuming that all chains undergo an equal-force deformation, the representative hybrid chain of $\mathscr{N}$ segments of length $\mathscr{B}$ has the same expression of the standard f–λ relationship as stated in Eq. (1):

$$f = \frac{k_B T}{b} \mathscr{L}^{-1}\left(\frac{\lambda}{\sqrt{\mathscr{N}}}\right), \tag{3}$$

where $\mathscr{N}$ and $\mathscr{B}$ are defined as follows:

$$\mathscr{N} = \left[\frac{\sum_{i\in I} \phi_i N_i}{\sum_i \phi_i \sqrt{N_i}}\right]^2 \quad \text{and} \quad \mathscr{B} = \frac{\sum_{i\in I} \phi_i \sqrt{N_i}}{\sqrt{\mathscr{N}}} b\,. \tag{4}$$

The corresponding segments of length $\mathscr{B}$, to be distinguished from the Kuhn segments, shall be referred to as *representative segments* because of their dependency on the chain-length distribution. The number $\mathscr{N}$ is the *characteristic number* of (representative) segments of the representative chain. Defining the *normalized stretch ratios* $\widehat{\lambda}_i$ and $\widehat{\lambda}$ as follows:

$$\forall i \in I, \quad \widehat{\lambda}_i := \frac{\lambda_i}{\sqrt{N_i}} \quad \text{and} \quad \widehat{\lambda} := \frac{\lambda}{\sqrt{\mathscr{N}}}\,, \tag{5}$$

where λ_i is the stretch ratio of the population i, the assumption of an equal-force deformation leads to an equality of the corresponding normalized stretch ratios:

$$\forall i, \quad \widehat{\lambda}_i = \widehat{\lambda}. \tag{6}$$

The integration of the response of this inhomogeneous representative chain over the unit sphere is not recalled here. It will be adapted to the semi-crystalline case in section 2.3.

2.1.3. Crystallization and melting

To define the crystallization of segments and stick with Flory's representation, crystallite sizes in loading direction and threshold stretch ratios of crystallization and of melting have to be known. They are defined in Part I of this work

(Gros et al., 2018) by using both classical theories of thermodynamics (considering changes in Gibbs free energy) and topological considerations. As depicted in Fig. 4 of Part I, crystallization occurs only if a spontaneously created critical nucleus is smaller than the space provided by the network, and instantaneous lateral growth follows before being stopped again by the allowed space. Melting occurs considering Gibbs free energy of a crystallite with finite sizes. A brief recall of the main assumptions and equations are given hereby.

Topological constraints (entanglements and crosslinks) are assumed to be physical fixed points lying along the chain, splitting it into subchains, denoted here as *1D meshes* and characterized by their number of Kuhn segments N^{topo}. With the hypotheses that each chain deforms in an affine manner, that topological constraints are aligned with the loading direction, and that the crystallite chain direction and the loading direction are the same, the end-to-end distance between two topological constrains can be calculated as described in Appendix A. From Eq. (13) of Part I, the stretch ratio λ_{ci} at which crystallization occurs in a network of N_i-chains is therefore defined as:

$$\lambda_{ci} = \underset{\lambda_i>0}{\arg\min} \left[\frac{4\gamma^{(1)}}{\left(1-\dfrac{T}{T_f^0}\right)\Delta H_f - T\Delta S_{\text{def}}(N_i,\lambda_i)} - \lambda_i \frac{N_i^{\text{topo}}}{\sqrt{N_i}} b \leqslant 0 \right] . \tag{7}$$

where $\gamma^{(k)}$ is the interface energy related to the crystal/amorphous interface whose normal direction is (k) ($k \in \{1,2,3\}$ referring to the principal directions of deformation) and assumed to be independent of the chain length, ΔH_f and T_f^0 are the melting enthalpy and melting temperature for an infinite crystal, $\Delta S_{\text{def}} = S(N_i,\lambda_i) - S(N_i,1)$ is the entropy induced by the deformation of the network, depending on N_i and λ_i and which can be expressed using statistical mechanics of polymer chains (Flory, 1953). The expressions used in this work is those related to Eq. (1) (Treloar, 1975):

$$S(N_i,\lambda_i) = \frac{\rho N_A}{N_i M_0}\left[S_{\text{ch}}(N_i,\lambda_i) + 2S_{\text{ch}}(N_i,\lambda_i^{-1/2})\right] \tag{8}$$

and:

$$S_{\text{ch}}(N_i,\lambda_i) = -k_B N_i \left[\widehat{\lambda}_i \mathcal{L}^{-1}\left(\widehat{\lambda}_i\right) + \ln \frac{\mathcal{L}^{-1}\left(\widehat{\lambda}_i\right)}{\sinh \mathcal{L}^{-1}\left(\widehat{\lambda}_i\right)}\right] \tag{9}$$

where $\widehat{\lambda}_i = \lambda_i/\sqrt{N_i}$ and $\rho N_A/(N_i M_0)$ is the number of chains in the considered system. N_A is the Avogadro number, ρ the material density and M_0 the molecular weight of one Kuhn segment. Subscripts i indicate that this definition can be applied to any population i taken separately. λ_{ci} corresponds to the stretch ratio at which a critical nucleus becomes smaller than the space allowed by the surrounding topological constraints which act as barriers to nucleation and crystallization, as represented in Fig. 4 of Part I. Once the crystallite is

formed, lateral growth follows but is limited again by topological constraints. The corresponding final sizes $\breve{L}_i$ of the parallelepipedic crystallite are:

$$\breve{L}_i^{(k)} = \begin{cases} \lambda_{ci} \dfrac{N_i^{\text{topo}}}{\sqrt{N_i}} b & \text{when} \quad k = 1\,, \\ \dfrac{1}{\sqrt{\lambda_{ci}}} \sqrt{N_i} b & \text{when} \quad k \in \{2,3\}\,. \end{cases} \tag{10}$$

Melting point is characterized by the cancellation of Gibbs free energy for a crystallite whose dimensions $\breve{L}_i^{(k)}$ ($k \in \{1,2,3\}$) are given. The stretch ratio λ_{mi} at which such stable crystallite melts is thus the solution of the following equation:

$$\sum_{k=1}^{3} \frac{2\gamma^{(k)}}{\breve{L}_i^{(k)}} - \left(1 - \frac{T}{T_f^0}\right) \Delta H_f + T \Delta S_{\text{def}}(N_i, \lambda_{mi}) = 0\,. \tag{11}$$

Given the characteristics of the populations including their N_i^{topo}, this section provides, for each population i, the crystallization stretch ratio λ_{ci} at which crystallization occurs, the dimensions ($\breve{L}_i^{(1)}$ in the loading direction in particular) of such stable crystallite, and the melting stretch ratio λ_{mi} at which corresponding melting occurs. These are sufficient to achieve the step (b) of the enrichment of Flory's chain.

2.2. Semi-crystallized representative chain

2.2.1. Semi-crystallized single chain and equivalent induced population

In Flory's representation of a semi-crystallized chain, a crystallite on a chain is represented as a few successive Kuhn segments aligned in the loading direction, as depicted in Fig. 2. Thus, a chain of N segments among which N_c segments crystallize, results in one or two subchains separated by a crystalline portion of N_c segments. However, the foregoing crystallization conditions require a different representation of a semi-crystallized chain. Indeed, according to our nucleation condition, a crystallite forms in each amorphous 1D mesh between two entanglements, meaning that there are as many crystallites as 1D meshes on a single chain. A semi-crystallized chain is thus here defined as a succession of 1D meshes (separated by entanglements), each following Flory's representation of a semi-crystallized chain.

In order to characterize this chain, let us first consider a single 1D mesh undergoing crystallization: when an initial N^{topo}-chain crystallizes, the crystallite of N_c segments can form at any position along the 1D mesh (at the middle, at one end, etc.), resulting in two "sub-chains", respectively of N_{sub1} and N_{sub2} segments, so that $N_{\text{sub1}} + N_c + N_{\text{sub2}} = N^{\text{topo}}$ as depicted in Figure 3 ("amorphous mesh" and "crystallized mesh"). These positions are assumed to be equiprobable. Systematically defining a random position along the chain and manage the behavior of all these new subchains might be heavy to compute. Another idea consists in assuming that the average position is in the middle of the chain and in splitting it into two equal parts, so that $N_{\text{sub1}} = N_{\text{sub2}} = (N^{\text{topo}} - N_c)/2$.

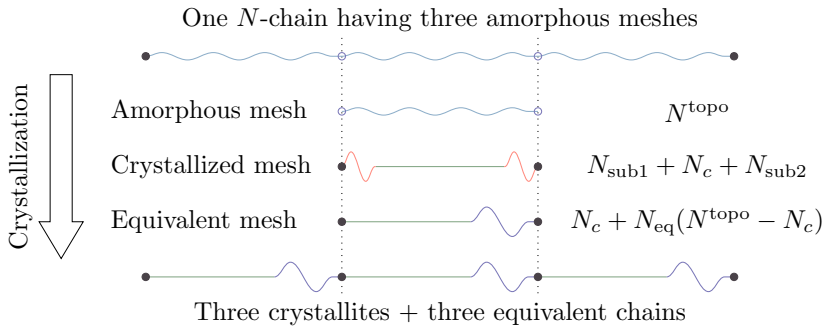

Figure 3: Steps for defining an equivalent chain.

This usual hypothesis (Mistry and Govindjee, 2014), although easy to manage, has the disadvantage that the average response (f–λ relationship) of the subchains is not necessarily the one of a chain defined by the arithmetic average of the numbers of segment. To conciliate these two aspects of simplicity and of respect of f–λ relationship, results of section 2.1.2 (Eq. (4)) are used to define an equivalent chain which reproduce the response of the assembly of the two subchains. In other words, extending this idea, a whole N-chain (having N/N^{topo} meshes) which crystallizes becomes a set of N/N^{topo} crystallites and of N/N^{topo} equivalent chains having $N_{\text{eq}}(N_{\text{sub}})$ segments each, this number of segments being defined as follows:

$$\sqrt{N_{\text{eq}}(N_{\text{sub}})} = \frac{\sum_{p=0}^{N_{\text{sub}}} N_{\text{sub}}}{\sum_{p=0}^{N_{\text{sub}}} (\sqrt{p} + \sqrt{N_{\text{sub}} - p})} = \frac{(N_{\text{sub}}+1)N_{\text{sub}}}{2} \left[\sum_{p=0}^{N_{\text{sub}}} \sqrt{p}\right]^{-1} \tag{12}$$

where $N_{\text{sub}} = N^{\text{topo}} - N_c$. Intermediate steps to obtain this equation are given in Appendix B. The equivalent mesh is depicted in Fig. 3. Equivalent chains induced by the crystallization of a given population constitute thus another population referred to as the *equivalent induced population*, which can potentially crystallize again if the conditions are met. Because of the average, a new associated segment length should be calculated each time (Eq. (4)). However, their computation showing that they vary between b and $0.88b$ when N_{sub} varies from 1 to 40 and considering the fact that our longest amorphous 1D meshes will contain only around 30 to 40 segments, the equivalent segment is approximated to b for the sake of simplicity of further equations, keeping in mind that this leads to a small overestimation of the length of the amorphous portion in a semi-crystallized representative chain.

2.2.2. Derivation of the heterogenous representative chain response

The semi-crystallized representative chain is composed by populations of chains, which can be semi-crystallized or totally amorphous. In Figure 4(a), a

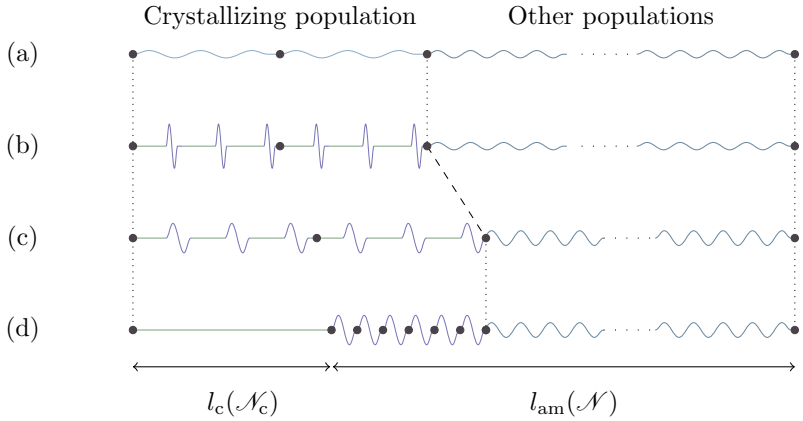

Figure 4: Representation of a semi-crystallized representative chain, having here initially several amorphous populations (a), one of which crystallizes (b). The chain instantaneously reaches its equilibrium (c). The crystallized segments are gathered at one chain end, forming a heterogeneous representative chain having a crystalline portion and a unique amorphous and inhomogeneous portion (d).

fully amorphous representative chain is represented, with one population (having two chains) isolated for description. Let us consider that the stretch ratio of the representative chain is so that threshold of crystallization of the isolated population is reached. From the previous section, the semi-crystallized population can be separated into crystallites (aligned segments) and the same amount of amorphous equivalent chains, as represented in Fig. 4(b) and (c), respectively before and after equilibrium. Let us mention that this equilibrium step induces a force decrease for the chains of other populations as in Flory's theory, but a stretching of the equivalent induced chains of the crystallizing population. The induced amorphous equivalent chains form an equivalent induced population, and furthermore, the position of the aligned crystallized segments does not matter from the viewpoint of the f–λ relationship of the whole chain: it is equivalent to gather all them (including those from different semi-crystallized populations) at one end of the representative chain, as represented in Fig. 4(d). The semi-crystallized representative chain is thus comprised of a single amorphous portion (amorphous part of the representative chain) constituted by all the amorphous chains (from equivalent induced populations and amorphous populations), and a single crystallized portion. The characteristic number $\mathscr{N}$ of the amorphous portion can be calculated by Eq. (4) because the hypothesis of an equal-force deformation still holds. The crystalline portion has $\mathscr{N}_c$ segments, equal to the sum of the crystallized segments of all semi-crystallized populations, converted into the number of representative segments of length $\mathscr{B}$

by means of Eq. (4):

$$\mathscr{N}_c = N_c \frac{b}{\mathscr{B}}. \tag{13}$$

Let us remark that the definitions of $\mathscr{N}$ and $\mathscr{N}_c$ are so that in general $\sqrt{\mathscr{N}} + \sqrt{\mathscr{N}_c} \neq \sqrt{\mathscr{N}^{\{0\}}}$ and $\mathscr{N} + \mathscr{N}_c \neq \mathscr{N}^{\{0\}}$, where $\mathscr{N}^{\{0\}}$ is the characteristic number of segments of the representative chain in its initial state. The superscript $\{0\}$ will be used to indicate that the quantity is considered at the initial state of the chain, when no population is crystallized.

The global stretch ratio of the semi-crystallized representative chain can be expressed using the same definition as for an amorphous representative chain, by addition of the end-to-end distances:

$$\lambda = \frac{\ell_{\text{am}} + \ell_c}{\ell_0} = \frac{\lambda_{\text{am}} \sqrt{\mathscr{N}} \mathscr{B} + \mathscr{N}_c \mathscr{B}}{\sqrt{\mathscr{N}^{\{0\}}} \mathscr{B}} = \frac{\lambda_{\text{am}} \sqrt{\mathscr{N}} + \mathscr{N}_c}{\sqrt{\mathscr{N}^{\{0\}}}} \tag{14}$$

where ℓ_{am} is the end-to-end distance of the amorphous portion of the representative chain, ℓ_c that of the crystalline portion, and ℓ_0 that of the chain in its undeformed initial state. This expression especially allows, given the global stretch ratio λ and knowing $\mathscr{N}$, $\mathscr{N}^{\{0\}}$ and $\mathscr{N}_c$, to express the stretch ratio λ_{am} of the amorphous portion. Let us mention that $\mathscr{N}$ and $\mathscr{N}_c$ depend on the considered state of the network (*i.e.* on crystallization progress), and that the representation of this semi-crystallized representative chain is, thanks to the conversion to the characteristic numbers of segments, similar to that of the usual semi-crystallized chain of Flory.

The crystalline degree χ_c of the representative chain can naturally be defined as the ratio of the number of crystallized segments to the total number of segments:

$$\chi_c = \frac{\mathscr{N}_c}{\mathscr{N}^{\{0\}}}\,, \tag{15}$$

and the complementary quantity which is the amorphous fraction $\chi_{\text{am}} = \mathscr{N}/\mathscr{N}^{\{0\}}$ considered by Flory (1947) in his semi-crystallized chain model.

Remark 2. *The theory proposed by Albouy and Sotta (2015) also suggests (after basic algebraic manipulations of Eq.* (14)*) to define the following alternative crystalline degree* χ_c'*:*

$$\chi_c' = \frac{\sqrt{\mathscr{N}_c}}{\sqrt{\mathscr{N}^{\{0\}}}} = \sqrt{\chi_c} \tag{16}$$

In fact, this quantity corresponds in our model as the ratio of the end-to-end distance of an undeformed $\mathscr{N}_c$*-chain and the end-to-end distance of the initial* $\mathscr{N}^{\{0\}}$*-chain.*

The characteristic number of segments of a representative chain not being equal to the simple sum of the Kuhn segments, let us link the previous quantities with the "real" mass crystalline degree, defined as the ratio of the numbers of Kuhn segments (sum of crystallized Kuhn segments divided by the total number of Kuhn segments), starting with the ratio of the amorphous segments and using

Eq. (4):

$$\frac{\sum \phi_i N_i}{\sum \phi_i^{\{0\}} N_i} = \frac{\sqrt{\mathscr{N}} \sum \phi_i \sqrt{N_i}}{\sqrt{\mathscr{N}^{\{0\}}} \sum \phi_i^{\{0\}} \sqrt{N_i}} = \Phi_{\text{am}} \sqrt{\frac{\mathscr{N}}{\mathscr{N}^{\{0\}}}} = \Phi_{\text{am}} \sqrt{\chi_{\text{am}}} \tag{17}$$

where:

$$\Phi_{\text{am}} := \frac{\sum \phi_i \sqrt{N_i}}{\sum \phi_i^{\{0\}} \sqrt{N_i}} \tag{18}$$

is the ratio between the end-to-end distances of the amorphous portion of the chain in an *undeformed* state, and the *undeformed* whole representative chain. We can observe that the quantity $\sqrt{\mathscr{N}/\mathscr{N}^{\{0\}}}$ appears quite naturally and that Φ_{am} is somewhat a quantity allowing to convert the "real" amorphous fraction into the end-to-end distances of representative segments. In a similar way, since $\mathscr{N}_c$ is defined as being equal to the sum of the N_c crystallized Kuhn segments converted into representative segments, the mass crystalline degree can be expressed as follows:

$$\frac{N_c}{\sum \phi_i^{\{0\}} N_i} = \frac{\mathscr{N}_c \mathscr{B}/b}{\sum \phi_i^{\{0\}} N_i} = \frac{\mathscr{N}_c \sum (\phi_i^{\{0\}} \sqrt{N_i})}{\sqrt{\mathscr{N}^{\{0\}}} \sum \phi_i^{\{0\}} N_i} = \sqrt{\frac{\mathscr{N}_c}{\mathscr{N}^{\{0\}}}} \sqrt{\frac{\mathscr{N}_c}{\mathscr{N}^{\{0\}}}} = \Phi_c \sqrt{\frac{\mathscr{N}_c}{\mathscr{N}^{\{0\}}}} = \Phi_c \sqrt{\chi_c} \tag{19}$$

where the quantity $\sqrt{\mathscr{N}_c/\mathscr{N}^{\{0\}}}$ appears, "adjusted" by the ratio Φ_c of the end-to-end distances of the crystallized portion which would be in an *undeformed* state, to the *undeformed* whole representative chain.

Remark 3. *Quantities such as ϕ_i, $\mathscr{N}$, $\mathscr{N}_c$ and χ_c evolve each time, but also only if, a population crystallizes or melts. Extending the notation $\{0\}$ to the different states the chain encounters when crystallization and melting happen, we introduce the superscript $\{s\}$ to indicate that the quantity is that of the chain considered at its state numbered s (0 being the initial state). This notation will be recurrently used in the rest of this work, and its conveniency is explained in section 3.1.2 from the perspective of model implementation. From a physical point of view, it expresses the fact that strain-induced crystallization of a network can be seen as a succession of discrete states of the network. Besides, the state of a chain depends on its stretch ratio, itself depending on the orientation $\mathbf{u}$ of the chain in the material; when applicable, this dependency will be indicated as $\{s(\mathbf{u})\}$.*

2.3. Full mechanical model

The previous amorphous and semi-crystallized representative chains are now used as inputs for a full-network model (Wu and van der Giessen, 1993). The derivation of the constitutive equation of an inhomogeneous network remaining totally amorphous is already described in a previous work (Verron and Gros, 2017). Following the same approach, crystallization is introduced, considering that only the amorphous portions supply deformation energy.

Despite the volume change induced by crystallization because of the difference in density with the amorphous phase, the incompressibility hypothesis is kept, but has to be justified because crystalline density is higher than that of the amorphous phase. According to Wood and Bekkedahl (1946), the volume change for unvulcanized natural rubber crystallizing between -50 and 15°C is between 2 et 2.7 %. Knowing that crystallization is favored in that range of temperature (especially around -25°C), we can assume that the volume change is not larger for strain-induced crystallization (in which crystalline degree does not surpass 25 % in the studied conditions). Furthermore, Leitner (1955) suggests in 1955 that a crystalline degree of 10 % corresponds to 1 % of volume change, which also leads to a volume change of 2,5 % for the 25 % of crystalline degree induced by deformation. Finally, Smith and Hanna (1941) propose as a crystalline density of approximately 0.950 g/cm^3, while amorphous one is around 0.910 g/cm^3 Mark (2006). If a quarter of the initial volume crystallizes, the volume chain would theoretically be less than 1 %. Although the volume change is non zero, we can reasonably assume that natural rubber is incompressible, even in a semi-crystallized state.

Let us consider a material point assimilated to a unit sphere. Let $\mathbf{F}$ be the deformation gradient at this point; for a homogeneous, isotropic, hyperelastic and incompressible material, the corresponding nominal stress tensor, *i.e.* the first Piola-Kirchhoff stress tensor, is defined as (Holzapfel, 2003):

$$\mathbf{P} = -p\mathbf{F}^{-T} + \frac{\partial W}{\partial \mathbf{F}} \tag{20}$$

where p is the hydrostatic pressure induced by the incompressibility constraint $\det \mathbf{F} = 1$, $\mathbf{I}$ is the identity tensor 3×3 and W is the strain energy density per unit of undeformed volume. In the framework such as that of the *full-network* model, W is derived by integration of the one-dimensional strain energy $\bar{w}$ of each direction (each representative chain) on the unit sphere $\mathscr{S}$ (Wu and van der Giessen, 1993), which means:

$$W(\mathbf{F}) = \frac{1}{|\mathscr{S}|} \iint_{\mathscr{S}} \bar{w}(\lambda(\mathbf{u}))\, \mathrm{d}^2\Omega(\mathbf{u}) = \langle \bar{w}(\lambda) \rangle \tag{21}$$

where $\lambda(\mathbf{u})$ is the stretch ratio of the representative chain in each direction $\mathbf{u}$ in space, *i.e.* $\lambda(\mathbf{u}) = ||\mathbf{F}\mathbf{u}||$ for the affine assumption adopted here, and $\mathrm{d}^2\Omega$ is its solid angle. The notation $\langle \cdot \rangle$ is used to express an average value over the unit sphere: $\langle \cdot \rangle = \frac{1}{|\mathscr{S}|} \iint_{\mathscr{S}} \cdot\, \mathrm{d}^2\Omega$.

The derivative of W with respect to $\mathbf{F}$ required for the calculation of $\mathbf{P}$ can be written as follows:

$$\frac{\partial W}{\partial \mathbf{F}} = \left\langle \frac{\partial \bar{w}}{\partial \mathbf{F}} \right\rangle = \left\langle \frac{d\bar{w}}{d\lambda(\mathbf{u})} \frac{\partial \lambda(\mathbf{u})}{\partial \mathbf{F}} \right\rangle = \left\langle \frac{d\bar{w}}{d\lambda(\mathbf{u})} \frac{1}{\lambda(\mathbf{u})} \mathbf{F}\mathbf{u} \otimes \mathbf{u} \right\rangle = \mathbf{F} \left\langle \frac{d\bar{w}}{d\lambda(\mathbf{u})} \frac{1}{\lambda(\mathbf{u})} \mathbf{u} \otimes \mathbf{u} \right\rangle . \tag{22}$$

This needs the calculation of the derivative of $\bar{w}(\lambda)$, which is the weighted sum of those of the populations:

$$\bar{w}(\lambda) = n_0 \sum_{i \in I} \phi_i^{\{s\}} w_i(\lambda_i)\,, \tag{23}$$

where n_0 is the chain density, w_i is the energy induced by the deformation of a N_i-chain, and the exponent $\{s\}$ indicates that the quantity is taken at the adequate state of the network, changing with crystallization (see Remark 3 at the end of section 2.2.2). It is important here to note that ϕ_i evolves with deformation (justifying the notation $\phi_i^{\{s\}}$) and that the sum of ϕ_i is equal to 1 only in the totally amorphous case, at the state $\{0\}$. Furthermore, $n_0 \sum_{i\in I} \phi_i^{\{s\}} N_i$ is equal to the number of amorphous segments in the considered volume (amorphous populations and equivalent induced populations for semi-crystallized populations). The characteristic number of segments (evolving with crystallization) of the representative chain is noted $\mathscr{N}^{\{s\}}$. The stretch ratio of the amorphous portion λ_{am} appears in the derivative, which is then equal to:

$$\frac{d\bar{w}}{d\lambda} = n_0 \sum_{i\in I} \phi_i^{\{s\}} \frac{\partial w_i(\lambda_i)}{\partial \lambda} = n_0 \sum_{i\in I} \phi_i^{\{s\}} \frac{dw_i(\lambda_i)}{d\lambda_i} \frac{\partial \lambda_i}{\partial \lambda_{\text{am}}} \frac{\partial \lambda_{\text{am}}}{\partial \lambda} = n_0 \sum_{i\in I} \phi_i^{\{s\}} f\sqrt{N_i} b \frac{\sqrt{N_i}}{\sqrt{\mathscr{N}^{\{s\}}}} \frac{\sqrt{\mathscr{N}^{\{0\}}}}{\sqrt{\mathscr{N}^{\{s\}}}} \tag{24}$$

by invoking the equality of the normalized stretch ratios (Eq. (6)), and from Eq. (1):

$$\frac{dw_i}{d\lambda_i} = \frac{dw_i}{dl_i} \frac{dl_i}{d\lambda_i} = f\sqrt{N_i} b\,. \tag{25}$$

Thus, since the expression of f for this semi-crystallized chain is:

$$f(\mathscr{N}, \lambda) = \frac{k_B T}{b} \mathscr{L}^{-1}\left(\frac{\lambda_{\text{am}}}{\sqrt{\mathscr{N}^{\{s\}}}}\right), \tag{26}$$

it follows:

$$\frac{d\bar{w}}{d\lambda} = \frac{\sqrt{\mathscr{N}^{\{0\}}}}{\sqrt{\mathscr{N}^{\{s\}}}} \frac{n_0 \sum_{i\in I} \phi_i^{\{s\}} N_i}{\sqrt{\mathscr{N}^{\{s\}}}} k_B T \mathscr{L}^{-1}\left(\frac{\lambda_{\text{am}}}{\sqrt{\mathscr{N}^{\{s\}}}}\right) \tag{27}$$

which means, by means of the relationships established in Eq. (17) :

$$\frac{d\bar{w}}{d\lambda} = \Phi_{\text{am}}^{\{s\}} \frac{n_0 \sum_{i\in I} \phi_i^{\{0\}} N_i}{\sqrt{\mathscr{N}^{\{s\}}}} k_B T \mathscr{L}^{-1}\left(\frac{\lambda_{\text{am}}}{\sqrt{\mathscr{N}^{\{s\}}}}\right) \tag{28}$$

where $\Phi_{\text{am}}^{\{s\}}$ is defined in Eq. (18). This expression indicates that the strain energy of a semi-crystallized chain whose amorphous portion has $\mathscr{N}^{\{s\}}$ segments is equal that of a network of $\mathscr{N}^{\{s\}}$-chains and having the same total number of segments, taken at the adequate stretch ratio λ_{am} and weighted by the term $\Phi_{\text{am}}^{\{s\}}$ (which can be understood as a transposition to a "linear" fraction of the considered number of segments to the total number of Kuhn segments $n_0 \sum_{i\in I} \phi_i^{\{0\}} N_i$). This leads to the nominal stress tensor:

$$\mathbf{P} = -p\mathbf{F}^{-T} + \mathbf{F} \left\langle \Phi_{\text{am}}^{\{s(\mathbf{u})\}} \frac{n_0 \sum_{i\in I} \phi_i^{\{0\}} N_i}{\sqrt{\mathscr{N}^{\{s(\mathbf{u})\}}}} k_B T \frac{1}{\lambda(\mathbf{u})} \mathscr{L}^{-1}\left(\frac{\lambda_{\text{am}}(\mathbf{u})}{\sqrt{\mathscr{N}^{\{s(\mathbf{u})\}}}}\right) \mathbf{u}\otimes\mathbf{u} \right\rangle, \tag{29}$$

and the crystalline degree is simply:

$$\chi_{c,\text{tot}} = \langle \chi_c^{\{s(\mathbf{u})\}} \rangle. \tag{30}$$

From a practical viewpoint, and as it is the case in the fully amorphous case, the numerical integration of the stress is obtained by choosing an integration method picking particular points on the unit sphere (analytical integration also exists (Khiêm and Itskov, 2016)). Three of these methods are recalled and discussed by Verron (2015).

3. Algorithm

Considering long-term equilibrium state of crystallization for each deformation step, an intuitive algorithm from the derivation of the model would be the following.

1. Apply $\mathbf{F}$ to the unit sphere and compute the normalized stretch ratios $\lambda(\mathbf{u})$ of the representative chains in each direction $\mathbf{u}$ (which are discrete points defined by the chosen numerical integration method).
2. For each representative chain (*i.e.* each direction $\mathbf{u}$):
   (a) compute the dimensions of the 1D meshes and critical nuclei of each population;
   (b) apply crystallization and melting criteria (Eqs. (7) and (11)) and determine if crystallites form or melt in each population;
   (c) gather the results of all the populations and compute the new amorphous stretch ratio of the representative chain, its crystalline degree and characteristic number of segments.
3. Assembly the results from all the representative chains and deduce the nominal stress tensor and global crystalline degree (Eqs. (29) and (30)).

This algorithm naturally follows the steps of the previous sections, but is numerically costly to compute: there is no reason for the system to be in equilibrium after crystallization process, then solving it requires to loop the algorithm in order to check and correct the new system if necessary.

A wish of simplifying the algorithm leads to the possibility of making *off-line* calculations which considerably lighten the computation (it reduced the computation time of two orders of magnitude). Figure 5 depicts the general structure of an original algorithm, which consists (from the left side to the right), to compute first independently the stretch ratios of crystallization and melting for the populations, then, given a chain-length distribution, to characterize all the states the network undergoes (i.e. to define all the quantities marked by the exponent $\{s\}$ in Eq. (29)), and finally to call them (for each direction) each time a deformation gradient $\mathbf{F}$ is applied to the unit sphere. Detailed steps are given below.

Remark 4. *It is to note here that there is no explicit evolution law driving crystallization and melting during the deformation process ; it rather arises from the computation and is the result of populations switching successively from an amorphous state to a crystallized state (and vice-versa for melting). This switch is triggered by reaching the threshold stretch ratios of crystallization and melting.*

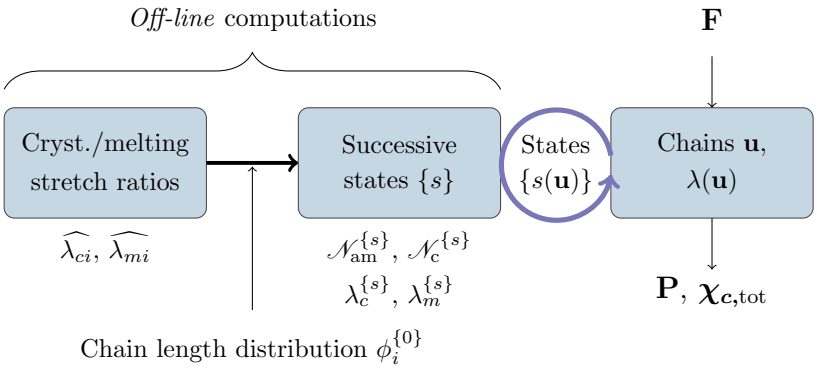

Figure 5: Dedicated algorithm.

3.1. Off-line computations

3.1.1. Crystallization and melting stretch ratios

From the way phase transition criteria were defined, the crystallization and melting stretch ratios of a population only depend on itself (local stretch ratio and end-to-end distance of its 1D mesh): their threshold stretch ratios λ_{ci} and λ_{mi}, as well as the number of segments of their crystallites, can be determined without knowing the chain-length distribution. The assumption of equal-force in chains indicating that at a given deformation of the representative chain, all the populations have the same normalized stretch ratios (Eq. (6)), it is convenient to use normalized stretch ratios here. Therefore, using Eqs. (7) and (11), $\widehat{\lambda_{ci}}$ and $\widehat{\lambda_{mi}}$ are computed for all $i \in I$.

3.1.2. Successive states of a representative chain

The originality of this algorithm lies in the reasoning presented here, where the knowledge of $\mathbf{F}$ is still not required.

The previous threshold normalized stretch ratios provide the order in which populations crystallize or melt. We can thus define the successive states of the system, characterized by the knowledge of the crystallized/amorphous state of all populations. The successive states {0}, {1}, {2}, {3},... are denoted by the notation $\{s\}$. Defining by 1 the crystallized nature of a population and 0 its amorphous nature, a matrix $\boldsymbol{c}$ can be built such that the component on line $s+1$ and column i, denoted $c_i^{\{s\}}$, indicates whether the population i is crystallized in the state $\{s\}$, as illustrated in Figure 6 with six populations N_1, N_2, N_3, N_4, N_5 and N_6. We shall assume that the melting order is the inverse of that of crystallization (which will be the case for the chosen parameters), which allows to keep the same matrix in the two processes. Let us also define similarly the matrix $\bar{\boldsymbol{c}}$, whose elements are equal to 0 if the population is crystallized and 1 if it is amorphous (contraposition of $\boldsymbol{c}$ in terms of logic). These boolean matrices ease computations by means of matrix manipulations. In these notations, the

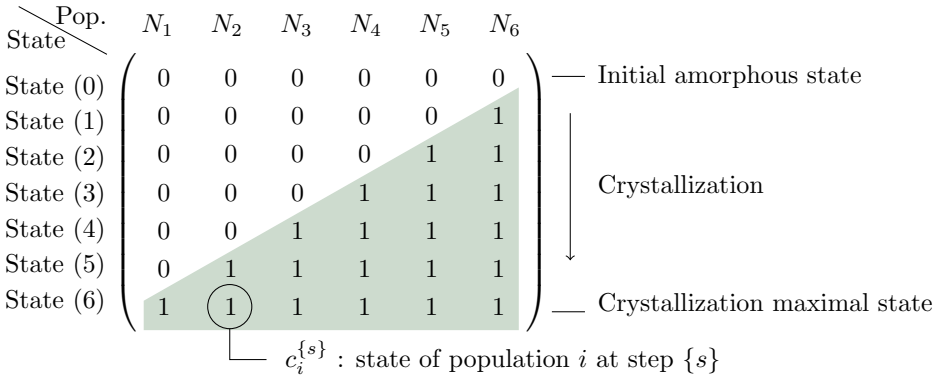

Figure 6: Example of a boolean matrix $\boldsymbol{c}$ indicating the states $c_i^{\{s\}}$ of a network of six populations i at each state $\{s\}$.

superscript $\{s\}$ of a value will indicate that it is taken at the state $\{s\}$ of the system ($\{0\}$ for the initial state).

The use of these matrices $\boldsymbol{c}$ and $\bar{\boldsymbol{c}}$ also allows to compute easily the successive chain-length distributions. A semi-crystallized population i produces equivalent induced chains of $N_{\mathrm{eq},i} := N_{\mathrm{eq}}(N_i^{\mathrm{topo}} - N_{ci})$ segments (Eq. (12)) in a quantity equal to the number of chains ϕ_i multiplied by the number $N_i/N_{\mathrm{eq},i}$ of 1D meshes in a chain. In the case where the longest chains crystallize first and ignoring a further crystallization of the equivalent induced populations, the chain-length distribution at a state $\{s\}$ is thus:

$$\begin{cases} \forall i \in I,\ \phi_i^{\{s\}} = \bar{\boldsymbol{c}}_i^{\{s\}} \phi_i^{\{0\}} \\ \text{then} \quad \forall i \in I,\ \phi_{\mathrm{eq},i}^{\{s\}} = \phi_{\mathrm{eq},i}^{\{0\}} + \boldsymbol{c}_i^{\{s\}} \phi_i^{\{0\}} N_i / N_i^{\mathrm{topo}} \,, \end{cases} \tag{31}$$

where $\phi_{\mathrm{eq},i}^{\{s\}}$ is the quantity of $N_{\mathrm{eq},i}$-chains. Let us mention that chain-length distribution (even the initial one) is introduced only here, and precise that if $\sum_{i\in I} \phi_i^{\{0\}} N_i$ represents the total number of segments in the system (with $\sum_{i\in I} \phi_i^{\{0\}} = 1$), $\sum_{i\in I} \phi_i^{\{s\}} N_i$ is the number of un-crystallized segments in the system at state $\{s\}$: the total number of segments being constant in the considered volume when changing from a state to another, ϕ shall not be normalized.

At each state $\{s\}$, the chain-length distribution is known, along with the number of crystallized segments for each population (number of 1D meshes in a chain N_i/N_i^{topo}, multiplied by the number of segments N_{ci} in a crystallite), and hence the characteristic numbers of the representative chain:

$$\mathscr{N}_c^{\{s\}} = \left[\sum_{i\in I} \left(c_i^{\{s\}} \phi_i^{\{0\}} N_{ci} \frac{N_i}{N_i^{\mathrm{topo}}} \right) \right] \left[\sum_{i\in I} \frac{\phi_i^{\{0\}} \sqrt{N_i}}{\sqrt{\mathscr{N}^{\{0\}}}} \right]^{-1} , \tag{32}$$

(where the last term converts Kuhn segments to representative segments) and

$$\mathscr{N}^{\{s\}} = \left[\sum_{i\in I} \varphi_i^{\{s\}} \sqrt{N_i}\right]^2 \quad \text{with} \quad \varphi_i^{\{s\}} = \frac{\phi_i^{\{s\}}\sqrt{N_i}}{\sum_{i\in I}\phi_i^{\{s\}}\sqrt{N_i}}\,. \tag{33}$$

The crystalline degree of the representative chain (discussed further in 4.5) is thus:

$$\chi_c^{\{s\}} = \mathscr{N}_c^{\{s\}}/\mathscr{N}^{\{0\}}\,. \tag{34}$$

Given the number of crystallized segments, the global stretch ratio is computed thanks to Eq. (14). In particular, we can define the global threshold stretch ratios $\lambda_c^{\{s\}}$ and $\lambda_f^{\{s\}}$ for *entering* and *leaving* a state $\{s\}$ using the equality of the normalized stretch ratios (Eq. (6)). In fact, if the state $\{s\}$ corresponds to the crystallization of the population $\bar{s}$, it follows:

$$\lambda_c^{\{s\}} = \frac{\widehat{\lambda_{c\bar{s}}}\mathscr{N}^{\{s-1\}} + \mathscr{N}_c^{\{s-1\}}}{\sqrt{\mathscr{N}^{\{0\}}}}\,, \tag{35}$$

where $\widehat{\lambda_{c\bar{s}}}$ is the normalized threshold stretch ratio of crystallization of population $\bar{s}$. In a similar way:

$$\lambda_m^{\{s\}} = \frac{\widehat{\lambda_{m\bar{s}}}\mathscr{N}^{\{s\}} + \mathscr{N}_c^{\{s\}}}{\sqrt{\mathscr{N}^{\{0\}}}}\,. \tag{36}$$

3.2. Semi-crystallized full-network model

All the pieces are ready to compute the 3D model. The deformation gradient $\mathbf{F}$ (brought in only at this stage) is firstly applied to the unit sphere in order to compute the stretch ratios $\lambda(\mathbf{u})$ of the representative chains in all the directions $\mathbf{u}$, characterized by the points of the chosen numerical integration method. Each chain having different state according to its direction, s depends on $\mathbf{u}$ and is denoted $s(\mathbf{u})$. The stretch ratio $\lambda(\mathbf{u})$ is compared to the global threshold stretch ratios in order to determine the state of the chain as detailed in the next paragraph. Once this state $\{s(\mathbf{u})\}$ is determined, the previous computations provide $\mathscr{N}^{\{s(\mathbf{u})\}}$ and $\mathscr{N}_c^{\{s(\mathbf{u})\}}$, allowing the computation of the stretch ratio of the amorphous part of the representative chain as follows:

$$\lambda_{\mathrm{am}}(\mathbf{u}) = \frac{\lambda(\mathbf{u})\sqrt{\mathscr{N}^{\{0\}}} - \mathscr{N}_c^{\{s(\mathbf{u})\}}}{\sqrt{\mathscr{N}^{\{s(\mathbf{u})\}}}}\,, \tag{37}$$

and all the quantities necessary to compute the nominal stress tensor are gathered. Global crystalline degree is simply defined as an arithmetic average of the crystalline degrees of the chains:

$$\chi_{c,\mathrm{tot}} = \frac{1}{U}\sum_{\mathbf{u}}^{U} \chi_c(\mathbf{u})^{\{s(\mathbf{u})\}}\,. \tag{38}$$

where U is the number of integration points in the unit sphere, *i.e.* the number of directions $\mathbf{u}$.

As for the remaining description of the determination of the new state of a semi-crystallized representative chain assumed to be at state $\{s_{\text{given}}\}$, let us consider a stretch ratio λ that applies on it. Note that it is not necessary to know if the deformation is a load or an unload. The comparison of λ with the threshold stretch ratios is a crucial part in the algorithm, which is done in two steps (whose order matters):

- λ is first compared to $\lambda_c^{\{s_{\text{given}}+1\}}$: if $\lambda \geqslant \lambda_c^{\{s_{\text{given}}+1\}}$, then the system changes to a more crystallized state $\{s\} = \{s_{\text{given}} + 1\}$ (moving down by one line in the matrix $\boldsymbol{c}$). The operation is iterated until $\lambda < \lambda_c^{\{s\}+1}$ or $\{s\} = \{s_{\max}\}$, with $\{s_{\max}\}$ being the most crystallized state reached by the system, *i.e.* the state where all the populations are crystallized. It corresponds to the last line of $\boldsymbol{c}$.

- If $\lambda < \lambda_c^{\{s_{\text{given}}+1\}}$, melting is tested: λ is compared to $\lambda_m^{\{s_{\text{given}}\}}$. If $\lambda \leqslant \lambda_f^{\{s_{\text{given}}\}}$, then the system changes to a less crystallized state $\{s\} = \{s_{\text{given}} - 1\}$ (moving up by one line in $\boldsymbol{c}$) and the operation is iterated until $\lambda > \lambda_m^{\{s\}}$ or $\{s\} = \{0\}$ (first line of $\boldsymbol{c}$).

If $\{s_{\text{given}}\} \geqslant \{s\}$, the deformation is a load (towards crystallization), and if $\{s_{\text{given}}\} < \{s\}$ then the deformation is an unload (towards melting).

Modeling the evolution of the network during a deformation path finally consists in discretizing the deformation history into steps of $\mathbf{F}$. Let us mention that the choice of the strain step (difference of global strain between each step, seen as data points in quasi-static experiment) is very particular in our model. Indeed, the state of the network can be calculated directly at any given strain level without any intermediate steps (to be considered carefully in unload processes); moreover, steps do not have to be small except in order to get a smooth curve. This is one of the greatest strength of the implementational aspects of the model, thanks to the proposed algorithm.

3.3. Summary of the new algorithm

A summary of the whole algorithm is proposed in Table 1.

Table 1: Summary of the algorithm (continued on next page).

(1) Crystallization and melting threshold stretch ratios.

Material constants (given): ρ, ΔH, M_0, b.
Parameters: relationship linking N to N^{topo}; T; γ; crystallization and melting conditions $(\mathscr{G}_c)$ and $(\mathscr{G}_f)$.
Inputs: (-)
Outputs: $\widehat{\lambda_{ci}}$, $\widehat{\lambda_{mi}}$, N_{ci} for all $i \in I$;
Key formulae:

· $\widehat{\lambda_{ci}}$ satisfying $(\mathscr{G}_c)$: $\dfrac{4\gamma^{(1)}}{\left(1-\frac{T}{T_f^0}\right)\Delta H_f - T\Delta S_{\text{def}}(N_i, \widehat{\lambda_{ci}})} - \widehat{\lambda_{ci}} N_i^{\text{topo}} b = 0\,.$ (Eq. (7))

· $\widehat{\lambda_{mi}}$ satisfying $(\mathscr{G}_f)$: $\displaystyle\sum_{k=1}^{3} \frac{2\gamma^{(k)}}{\breve{L}_i^{(k)}} - \left(1-\frac{T}{T_f^0}\right)\Delta H_f + T\Delta S_{\text{def}}(N_i, \widehat{\lambda_{mi}} N_i) = 0\,.$ (Eq. (11))

· $N_{ci} = \dfrac{\breve{L}_i^{(1)}}{b} = \widehat{\lambda_{ci}} N_i^{\text{topo}}\,.$ (Eq. (10))

(2) Definition and chain-length distribution of each state.

Parameters: $\left(\phi_i^{\{0\}}\right)_{i\in I}$ (initial number of N_i-chains in the considered volume).
Inputs: $\widehat{\lambda_{ci}}$, $\widehat{\lambda_{mi}}$.
Outputs: $\boldsymbol{c}$, $\bar{\boldsymbol{c}}$ and $(\phi_i^{\{s\}})_{i\in I}$ of each state {s}.
Key formulae:

· For each $\{s\}$ in $i \in I$, $c_i^{\{s\}} = 1$ if the population is crystallized, 0 otherwise.

· For each $\{s\}$ in $i \in I$, $\bar{c}_i^{\{s\}} = 0$ if the population is crystallized, 1 otherwise.

· $\forall i \in I$, $\phi_i^{\{s\}} = \bar{c}_i^{\{s\}} \phi_i^{\{0\}}$, and then $\phi_{\text{eq},i}^{\{s\}} = \phi_{\text{eq},i}^{\{0\}} + c_i^{\{s\}} \phi_i^{\{0\}} \dfrac{N_i}{N_i^{\text{topo}}}$ where $\phi_{\text{eq},i}^{\{s\}}$ is the quantity of chains having $N_{\text{eq},i} = N_{\text{eq}}(N_i^{\text{topo}} - N_{ci})$ segments. (Eq. (31))

(3) Quantities associated to each state.

Parameters (already introduced): $\left(\phi_i^{\{0\}}\right)_{i\in I}$ and relationship linking $N \mapsto N^{\text{topo}}$.

Inputs: $\widehat{\lambda_{ci}}$, $\widehat{\lambda_{mi}}$, N_{ci}, $\boldsymbol{c}$.
Outputs: $\lambda_c^{\{s\}}$, $\lambda_m^{\{s\}}$, $\mathscr{N}_c^{\{s\}}$, $\mathscr{N}^{\{s\}}$, $\chi_c^{\{s\}}$.
Key formulae:

- $\lambda_c^{\{s\}} = \dfrac{\widehat{\lambda_{c\bar{s}}}\mathscr{N}^{\{s-1\}} + \mathscr{N}_c^{\{s-1\}}}{\sqrt{\mathscr{N}^{\{0\}}}}$ and $\lambda_f^{\{s\}} = \dfrac{\widehat{\lambda_{m\bar{s}}}\mathscr{N}^{\{s\}} + \mathscr{N}_f^{\{s\}}}{\sqrt{\mathscr{N}^{\{0\}}}}$ where $\widehat{\lambda_{c\bar{s}}}$ and $\widehat{\lambda_{m\bar{s}}}$ are the threshold stretch ratios of crystallization and melting of population $\bar{s}$ which crystallizes (resp. melts) at state $\{s\}$. (Eqs. (14), (35), and (36))

- $\mathscr{N}_c^{\{s\}} = \left[\sum_{i\in I}\left(c_i^{\{s\}}\phi_i^{\{0\}}N_{ci}\dfrac{N_i}{N_i^{\text{topo}}}\right)\right]\left[\sum_{i\in I}\dfrac{\phi_i^{\{0\}}\sqrt{N_i}}{\sqrt{\mathscr{N}^{\{0\}}}}\right]^{-1}$. (Eq. (32))

- $\mathscr{N}^{\{s\}} = \left[\sum_{i\in I}\varphi_i^{\{s\}}\sqrt{N_i}\right]^2$ where $\varphi_i^{\{s\}} = \dfrac{\phi_i^{\{s\}}\sqrt{N_i}}{\sum_{i\in I}\phi_i^{\{s\}}\sqrt{N_i}}$. (Eq. (33))

- $\chi_c^{\{s\}} = \mathscr{N}_c^{\{s\}}/\mathscr{N}^{\{0\}}$. (Eq. (34))

(4) Representative chain.

Parameters: (-)
Inputs: λ and a state $\{s_{\text{given}}\}$ of the system.
Outputs: the updated state $\{s\}$ and the amorphous stretch ratio λ_{am} corresponding to λ at this state.
Key formulae:

- Determination of the state:
  - If $\lambda \geqslant \lambda_c^{\{s_{\text{given}}+1\}}$, then $\{s\} = \{s_{\text{given}}+1\}$. Iterations until $\lambda < \lambda_c^{\{s+1\}}$ or $\{s\} = \{s_{max}\}$.
  - Otherwise : if $\lambda \leqslant \lambda_f^{\{s_{\text{given}}\}}$, then $\{s\} = \{s_{\text{given}}-1\}$. Iterations until $\lambda > \lambda_f^{\{s\}}$ or $\{s\} = \{0\}$.

- $\lambda_{\text{am}} = (\lambda\sqrt{\mathscr{N}^{\{0\}}} - \mathscr{N}_c^{\{s\}})/\sqrt{\mathscr{N}^{\{s\}}}$. (Eq. (37))

(5) *Full-network.*

Parameters: Numerical integration method and corresponding integration points on the unit sphere (ensemble U).
Inputs: deformation gradient $\mathbf{F}$.
Outputs: $\mathbf{P}$, $\chi_{c,\text{tot}}$.
Key formulae:

- $\lambda(\mathbf{u}) = ||\mathbf{F}\mathbf{u}||$ (giving $\{s(\mathbf{u})\}$ and $\lambda_{\text{am}}(\mathbf{u})$ from (4)).

- $\mathbf{P} = -p\mathbf{F}^{-T} + \mathbf{F}\left\langle \Phi_{\text{am}}^{\{s(\mathbf{u})\}}\dfrac{n_0\sum_{i\in I}\phi_i^{\{0\}}N_i}{\sqrt{\mathscr{N}^{\{s(\mathbf{u})\}}}}kT\dfrac{1}{\lambda(\mathbf{u})}\mathscr{L}^{-1}\left(\dfrac{\lambda_{\text{am}}(\mathbf{u})}{\sqrt{\mathscr{N}^{\{s(\mathbf{u})\}}}}\right)\mathbf{u}\otimes\mathbf{u}\right\rangle$ where $n_0\sum_{i\in I}\phi_i^{\{0\}}N_i$ is the total number of segments in one direction and $\Phi_{\text{am}}^{\{s(\mathbf{u})\}} = \dfrac{\phi_i^{\{s(\mathbf{u})\}}\sqrt{N_i}}{\sum\phi_i^{\{0\}}\sqrt{N_i}}$. (Eqs. (18) and (29))

- $\chi_{c,\text{tot}} = \dfrac{1}{U}\sum_{\mathbf{u}}^{U}\chi_c(\mathbf{u})^{\{s(\mathbf{u})\}}$. (Eq. (38))

4. Results and discussion

In this section, the model is illustrated considering a uniaxial experiment whose deformation gradient is:

$$\boldsymbol{F} = \begin{bmatrix} \lambda & 0 & 0 \\ 0 & 1/\sqrt{\lambda} & 0 \\ 0 & 0 & 1/\sqrt{\lambda} \end{bmatrix} . \tag{39}$$

We are interested in calculating the nominal stress tensor $\mathbf{P}$, particularly P_{11}, as a function of the applied λ and on the crystalline degree χ_c. We assume long-term equilibrium state of crystallization at each deformation step.

4.1. Numerical values and parameters

The numerical integration method proposed by Sloan and Womersley (2004) is chosen as suggested in a study by Verron (2015), with 441 integration points. Numerical values are $N_A \approx 6.02 \times 10^{23}$ mol^{-1}, $k_B \approx 1.38 \times 10^{-23}$ m$^2 \cdot$ kg $\cdot$ s$^{-2} \cdot$ K^{-1}, and finally for *cis*-1,4-polyisoprene, $b = 9.34$ Å, and $M_0 = 128.6$ g/mol, and $\rho = 0.91 \times 10^6$ g/mol^3 (Mark, 2006, 2009).

The parameters of the models and the way they are determined in this section are as follows.

- Chain-length distribution: a log-normal distribution, and a triangular distribution which can be seen as a rough approximation of the log-normal distribution, are considered. Both distributions are plotted in Figure 7(a). Their parameters are determined so that the mechanical response is in agreement with the part without crystallization, *i.e.* at low stretch ratios, of the experimental "target" curve.

- Distribution of the entanglements: poorly known and here supposed to be given, we use an approximate fit of simulation results conducted by Steenbakkers et al. (2014) (converted from real monomer to Kuhn segments):

$$N_i \longmapsto N_i^{\text{topo}} = \begin{cases} 17 + 20 \left[\dfrac{2}{\pi} \arctan\left(\dfrac{N_i}{50} \right) \right] & \text{if } N_i > 16\,, \\ N_i & \text{otherwise.} \end{cases} \tag{40}$$

  The corresponding graph is represented in Fig. 7(b).

- Interface energies σ_e and σ_l (or equivalently σ_e and the ratio $\alpha := \sigma_l/\sigma_e$): they are supposed constant because of a lack of knowledge about their evolution with respect to chain length, deformation and temperature, and adjusted so that the curves from the model are in good agreement with the experiments. An example is shown with variable interface energies to show the importance of their study. Used values are: $\sigma_e = 0.022$ when $N \leqslant 50$, increasing linearly to reach 0.03 when $N = 150$; $\alpha = \sigma_l/\sigma_e = 0.09$ when $N \leqslant 50$, decreasing linearly piecewise to reach 0.04 when $N = 90$ and 0.02 when $N = 115$, then staying constant.

(a)

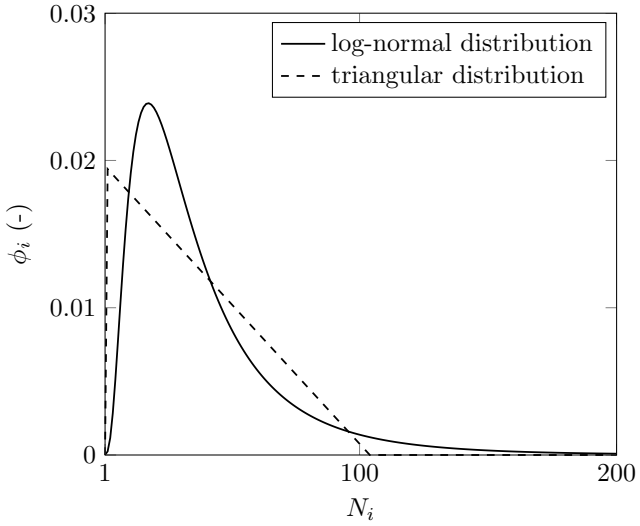

(b)

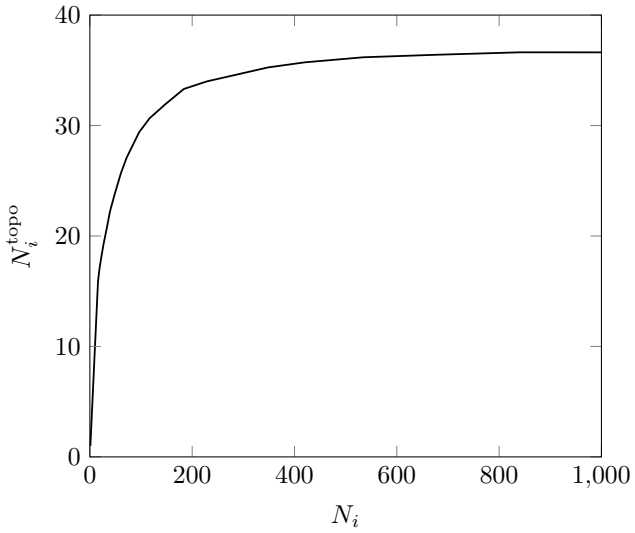

Figure 7: (a) Chain-length distributions used to plot the results: log-normal (solid) and triangular (dashed) distributions with parameters given in Table 2. (b) Distribution of entangle sed to plot the results (Eq. (40)).

4.2. Macroscopic crystalline degree and mechanical response

Figure 8 compares the curves of crystalline degree (a) and mechanical responses (b) of the whole unit sphere computed with the sets of parameters given in Table 2, obtained with isothermal conditions (21 ℃), superimposed

Table 2: Parameters used to plot the results for $T = 21$℃.

Distribution	Formulae	Parameters	σ_e	α
Log-normal	$N \mapsto \frac{1}{N\sqrt{2\pi}\delta} \exp\left(-\frac{(\ln N - \ln N_0)^2}{2\delta^2}\right)$	$N_0 = 30$, $\delta = 0.73$	0.026	0.035
Triangular	$N \mapsto \begin{cases} \frac{2(N-N_1)}{(N_3-N_1)(N_2-N_1)} & \text{when } N_1 \leqslant N < N_2 \\ \frac{2}{(N_3-N_1)} & \text{when } N = N_2 \\ \frac{2(N_3-N)}{(N_3-N_1)(N_3-N_2)} & \text{when } N_2 < N \leqslant N_3 \\ 0 & \text{otherwise} \end{cases}$	$N_1 = 1$, $N_2 = 2$, $N_3 = 104$	0.026	0.025
		$N_1 = 1$, $N_2 = 2$, $N_3 = 150$	(see text)	

to experimental results proposed by Albouy et al. (2012). In the experiments, natural rubber cured with 1.5 g of sulfur is indicated to have approximatively 75 monomers between two crosslinks, which is equivalent to 40 statistical Kuhn segments and to a network density 0.98 mol/cm^3. Stroboscopic X-ray measurements are obtained at 21 ℃ and at a deformation rate of $\dot{\lambda} = 0.0033$ s^{-1}.

First of all, it is to note that both chain length distributions (with constant interface energies) lead to similar results. For the three sets of parameters, the model captures qualitatively the experimental characteristics. Indeed, crystalline degree exhibits a threshold at $\lambda \approx 4$, followed by a smooth increase during all the loading process, and a decrease at unload accompanied by a hysteresis. As usually observed in experimental results, the corresponding mechanical response exhibits a slight plateau when crystallization starts, followed by a strengthening. The responses at load and unload coincide when crystalline degree comes back to zero, because the stress response at unload also present a hysteresis solely due to crystallization and melting.

It is also to note that the crystalline degree has not the same definition in our model, where only one direction of the crystallite is taken into account, and in the experimental measurement. In the modelled crystalline degree, a plateau at the beginning of the unload is visible when constant interface energies are used. This plateau does not exist in the experimental results plotted here, but does in the data of Toki et al. (2003) for a deformation at 0 ℃. In the model, it is due to the fact that threshold stretch ratio of melting (*i.e.* the melting point) is not close to the crystallization threshold, and consequently, significant unload is needed to reach it even for populations that have crystallized at the end of the load. Changing the interface energies allows to reduce this gap. Although they are not presented here, we also observe with our model a longer plateau

(a)

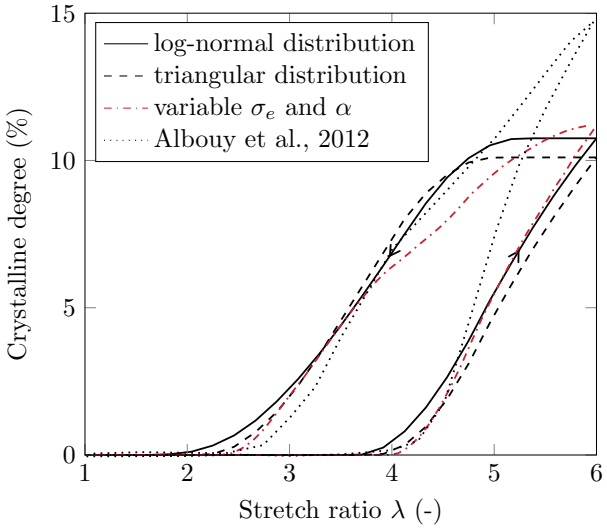

(b)

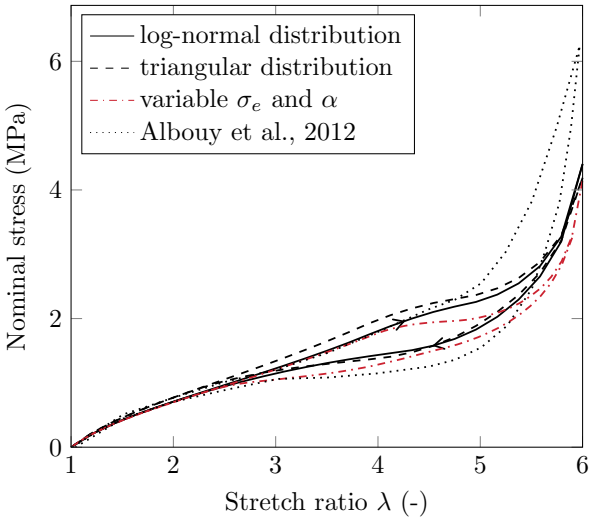

Figure 8: Crystalline degree curves (a) and mechanical responses (b) for a uniaxial loading. Experimental results from Albouy et al. (2012) are given in dotted lines, theoretical results with the log-normal distribution in solid line, and with the triangular distribution in dashed line.

when temperature decreases, which is experimentally observable and physically reasonable as the lower the temperature is, the more stable the crystallites are. Similarly, the model can qualitatively reproduce results showing that not all the crystallites are melt at the end of the unload.

From a quantitative perspective, a significant deviation is observed in mechanical response: the model overestimates the impact of crystallization on the remaining amorphous part. Indeed, our representation of a semi-crystallized chain assumes that crystallites are perfectly oriented in deformation direction, that chains never fold back into a same crystallite, and that all the 1D meshes crystallize. These three assumptions are acting in favor of a force decrease during crystallization. A parameter attenuating the impact of crystallization on mechanical response (a coefficient indicating a pourcentage of crystallizing 1D meshes for example) improves the results.

Despite these quantitative deviations, using few, simple, physically-based parameters allow to have a better analysis of the physics. and we choose, in the rest of the paper, to keep our physical approach avoiding a avoid phenomenological approach although we believe that it is possible, with further development of the code, to mathematically find optimized sets of parameters.

4.3. Network evolution

Crystallization and melting in the network naturally implies an evolution of chain-length distribution in each of the representative chains depending on their orientation in the sphere. Figure 9 provides, for a given initial condi-

Figure 9: Chain-length distribution evolution during crystallization.

tion, the changes in this distribution for some states during the loading process of one representative chain. The initial distribution is visible at the front of the plot. Longer chains crystallize first due to the assumption of equal-force deformation and definitions of threshold stretch ratios of crystallization, and then populations crystallize consecutively towards shorter chains. Because the induced populations never have chains longer than the 1D meshes, the populations seeing their number of chains increase are extremely short chains, whose crystallization threshold is never reached. The emerging sharp peak in short chain domain represents these induced populations having 1 to 36 segments according to Eq. (40).

These distributions allow to compute easily the characteristic number $\mathscr{N}^{\{s\}}$ of some representative chains during the deformation (their orientation in the unit sphere is described in the next section). Their evolution is plotted in Figure 10: since longer chains crystallize first, one can naturally observe that the average chain-length decreases while crystallization occurs. Depending on the direction of the chains and their applied stretch ratio, some reach their maximum crystalline degree, corresponding to the lower limit of possible $\mathscr{N}^{\{s\}}$, and remain at a same chain-length. This is consistent with the idea of a strengthening of the material despite of the existence of a force decrease following crystallization

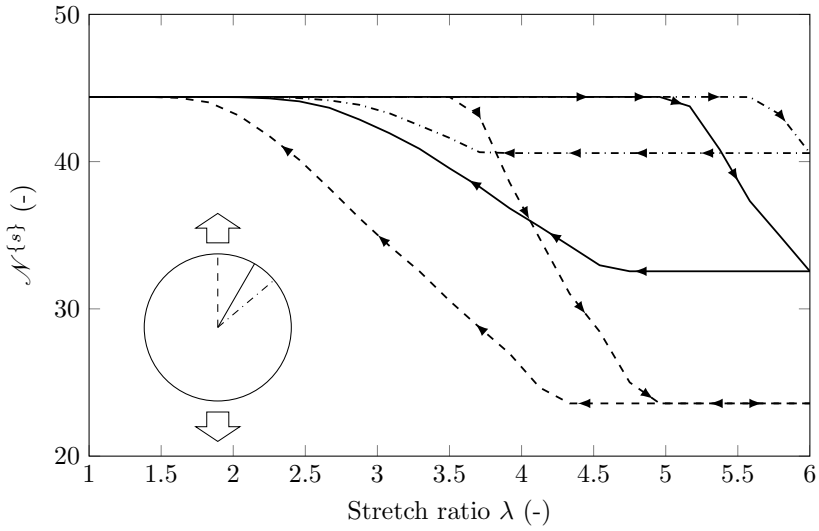

Figure 10: Evolution of the characteristic number $\mathcal{N}^{\{s\}}$ of the amorphous portion of representative chains having different orientations (0, 30 and 50° with loading direction as shown on the pictogram where loading direction is vertical), during load and unload with respect to the stretch ratio.

(depicted in Fig. 2): the competition between the two creates a plateau and then a steeper strengthening because the remaining amorphous part has become short. Furthermore, the hysteresis observed on the stress-strain curves are due to the difference of $\mathcal{N}^{\{s\}}$ at load and unload.

4.4. Evolution at the scale of the unit sphere

One peculiarity of this model, from its construction, is that the evolution of physical parameters can be observed, and that for each direction. In this section, physical quantities are therefore investigated, along with their dependency to orientation. From now on, all graphs are plotted using the log-normal distribution and corresponding parameters given in Table 2.

Evolutions of crystalline degree and forces in the chains are represented in Figures 11 and 12, as sets of points corresponding to some of the integration points. Their color indicates the values of crystalline degree, respectively force, of the corresponding representative chain. For the sake of visibility, spheres are represented undeformed but are taken at different stretch ratio (loading direction is vertical). Fig. 11 unsurprisingly indicates that crystallization occurs first in chains which are the most oriented towards loading direction. The effects on forces are straightforward given the derivation of the model and the previous observations.

Three zones can be defined: the pole (small angle Ψ of the chain with loading direction), a "crown" in which chains crystallize but at a weaker intensity, the equatorial zone, and finally an intermediate zone where chains do not crystallize.

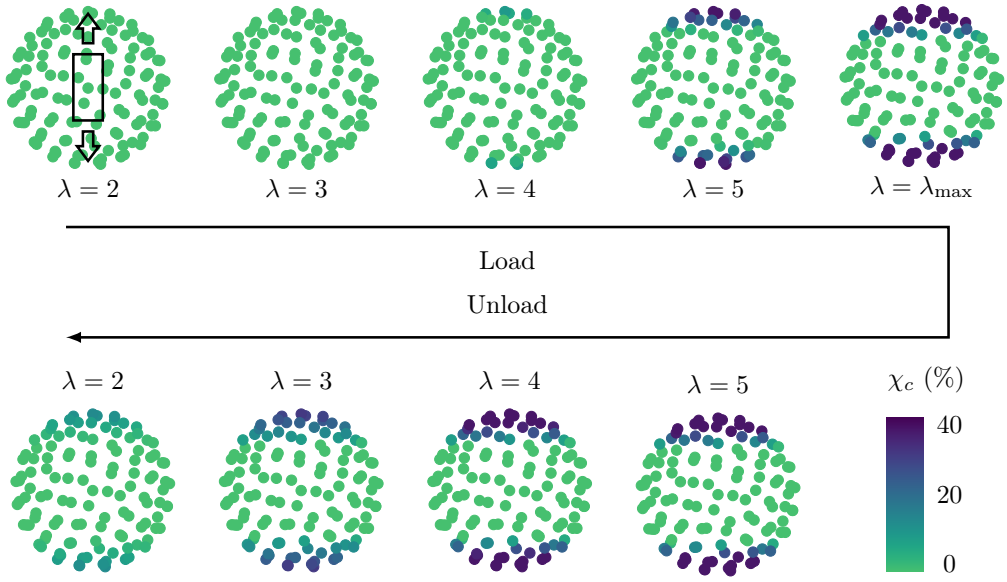

Figure 11: Evolution of crystalline degree in some representative chains of the *full-network* sphere. Loading direction is vertical.

A few chains are chosen to represent them in the following: $\Psi \approx 0°$ and $90°$ for the pole and equatorial zone, around $30°$ and $50°$ for the crown, and $70°$ for the intermediate zone.

4.5. Crystalline degree

Crystalline degree, corresponding to those quantified by colors in Fig. 11, is plotted in Figure 13 for the chosen representative chains. Only those of the pole and the crown are visible because the other chains remain amorphous. For the polar chain, it can be seen that crystalline degree reaches a maximum (at around $\lambda = 5$) and that it does not further evolve: the chain has reached its maximum state of crystallization.

4.6. Force decrease due to crystallization

The knowledge of the characteristic number of segments of a representative chain allows to deduce the normalized stretch ratio $\widehat{\lambda_{\text{am}}}$ of the amorphous part of the chain (amorphous stretch ratio divided by $\sqrt{\mathcal{N}\{s\}}$), represented in Figure 14(a) for the chosen representative chains. The most oriented chains are divided in two categories: those (most oriented) of which the amorphous extension seems to significantly increase after a slow down at crystallization, and those (less oriented) that stop before the steep increase. The following increase corresponds to the state at which crystallization has reached its maximum state

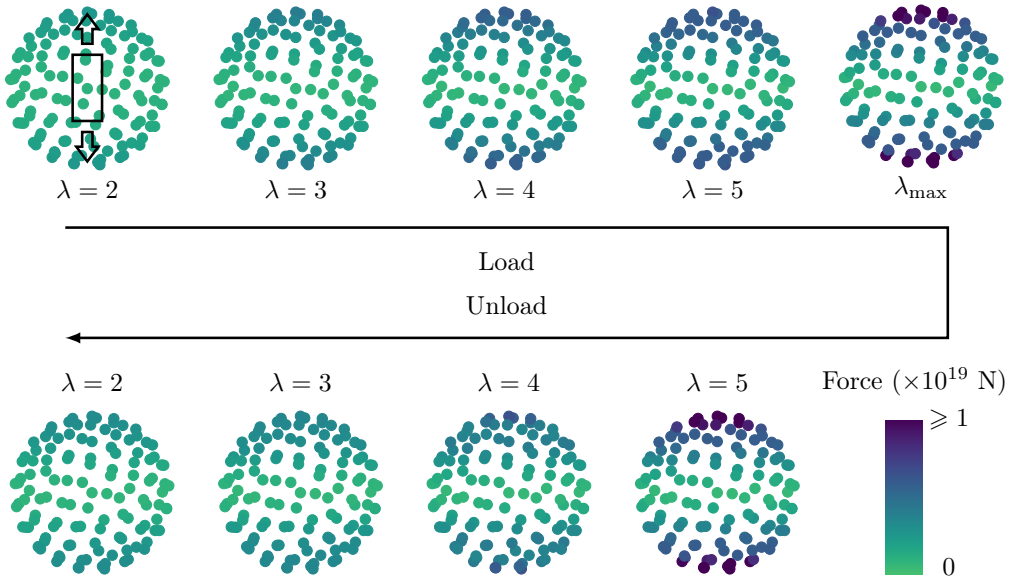

Figure 12: Evolution of force in some representative chains of the *full-network* sphere. Loading direction is vertical.

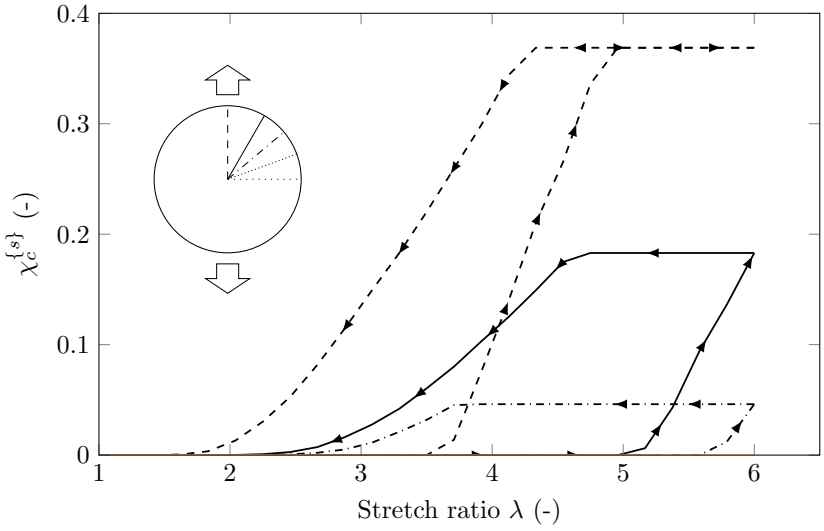

Figure 13: Crystalline degree of some representative chains having different orientations (as shown on the pictogram where loading direction is vertical) during load and unload with respect to the stretch ratio.

(a)

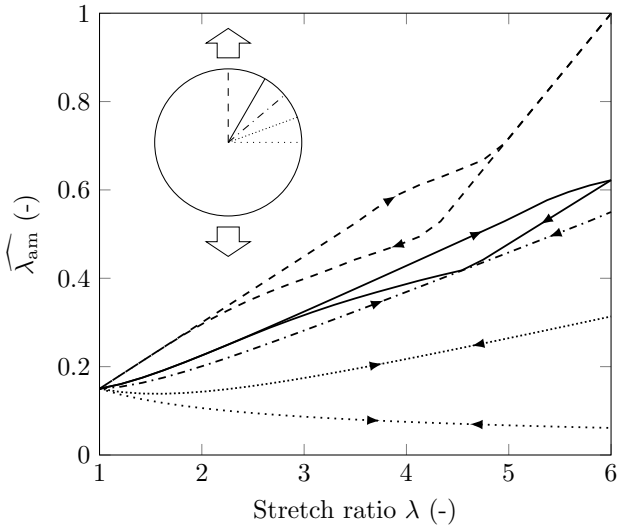

(b)

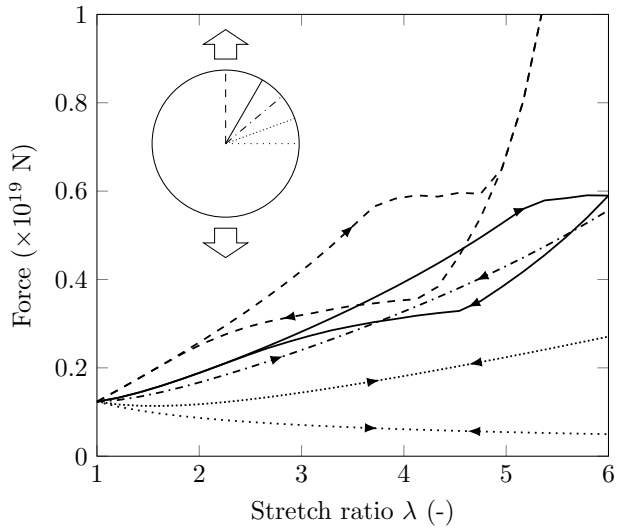

Figure 14: Normalized stretch ratio $\widehat{\lambda_{am}}$ (a) and force (b) of some representative chains (shown on the pictogram where loading direction is vertical) having different orientations between load and unload with respect to the stretch ratio.

in the representative chain: λ_{am} and λ are related by the linear relationship

$\lambda\sqrt{\mathscr{N}^{\{0\}}} = \lambda_{\text{am}}\sqrt{\mathscr{N}^{\{s\}}} + \mathscr{N}_c^{\{s\}}$ (Eq. (14)) where $\mathscr{N}^{\{0\}}$, $\mathscr{N}^{\{s\}}$ and $\mathscr{N}_c^{\{s\}}$ are constants when the state of the network does not change. Moreover, although it is difficult to define an average behavior, the chains from the pole and from the crown seem to reproduce and explain the experimental observations by Albouy et al. (2012) showing a peculiar behavior of the global amorphous stretch ratio. Indeed, the two plateaux at load and unload are expressed as the slow down of the evolution, and the steep increase can be assumed to be attenuated by the other less-oriented chains. Let us also look at the mechanical response of the chosen representative chains: Fig. 14(b) shows their force evolution (calculated from the amorphous stretch ratio of the semi-crystallized chain and its characteristic number of segments). The general tendency is as expected, and the hysteresis is clearly visible for the chains undergoing crystallization (Fig. 13). The plateaux, particularly visible in the loading process, are explained by the force decrease due to crystallization (Fig. 2).

4.7. Influence of the parameters

This section finally comments the influences model parameters: distribution of entanglements (*i.e.* length of 1D meshes), interface energies, and chain-length distribution. The model is very sensitive to these parameters, especially to interface energies. Table 3 summarizes the influence of the length of 1D meshes

Table 3: Influences of N^{topo}, γ_e and γ_l on thermodynamical quantities for a population. The second column shows the expressions used to determine the evolution. Indices i are omitted.

		$N^{\text{topo}}\nearrow$	$\gamma_e\nearrow$	$\gamma_l\nearrow$
λ_c	$= 4\gamma_e\sqrt{N}/(\Delta G_f(\lambda_c, N)N^{\text{topo}})$	$\searrow$	$\nearrow$	$\longrightarrow$
$L^{*(1)}$	$= -4\gamma_e/\Delta G_f(\lambda_c, N) = \widehat{\lambda_c}N^{\text{topo}}b$	$\nearrow$	$\nearrow$	$\longrightarrow$
$L^{*(2)}$	$(= L^{*(3)}) = L^{*(1)}\gamma_l/\gamma_e$	$\nearrow$	$\searrow$	$\nearrow$
$\breve{L}^{(1)}$	$= L^{*(1)}$	$\nearrow$	$\nearrow$	$\longrightarrow$
$\breve{L}^{(2)}$	$(= \breve{L}^{(3)}) = \sqrt{N/\lambda_c}b$	$\nearrow$	$\searrow$	$\longrightarrow$
$\sum(2\gamma^{(k)}/\breve{L}^{(k)})$	$= -\Delta G_f(\lambda_c, N)/2 + 4\gamma_l/\breve{L}^{(2)}$	$\searrow$	$\nearrow$	$\nearrow$
λ_f	(identical to the evolution of $\sum(2\gamma^{(k)}/\breve{L}^{(k)})$)	$\searrow$	$\nearrow$	$\nearrow$
$N_{c,ch}$	$= (L^{*(1)}/b) \times (N/N^{\text{topo}}) = \lambda_c\sqrt{N}$	$\searrow$	$\nearrow$	$\longrightarrow$
N_{f}	$= N^{\text{topo}} - \breve{L}^{(1)}/b = N^{\text{topo}}(1 - \widehat{\lambda_c})$	$\nearrow$	$\searrow$	$\longrightarrow$

and of interface energies on thermodynamical quantities for a given population. These results, often intuitive given the physics of crystallization or the model derivation, are guessed from the equations listed in the second column, and are observable in computed results.

As indicated in Table 3 (third column) and intuitively, crystallization happens later when 1D meshes are shorter. The size of formed crystallites depends again on the length of the 1D meshes; but at the scale of the chain, the number of crystallized segments is $\lambda_{ci}N_i$ and thus depends on N_i^{topo} only through λ_{ci}. The computation of the sizes of the stable crystallite, whose height does not change, also does not bring N^{topo} in, neither in melting except through the height of the crystallite (a larger crystallite is, in fact, more stable). The entanglements of each population i thus just increase or decrease λ_{ci}, and then λ_{mi} in consequence. Moreover, if crystallite size decreases, the equivalent induced populations have longer chains, leading to a larger characteristic number $\mathscr{N}$ of segments in the amorphous portion of the representative chain.

Interface energies are crucial in the determination of crystallization and melting conditions; let us distinguish here the lateral interface energies γ_l ($\gamma^{(2)}$ and $\gamma^{(3)}$) and the end surface interface energy γ_e ($\gamma^{(1)}$). Table 3 (fourth and fifth columns) summarizes the influence of γ_e and γ_l on the quantities related to crystallization and melting. From our crystallization condition, the crystallization threshold is reached later when γ_e increases. The lateral interface energies are then involved in the crystallite growth: when γ_l increases, the lateral sizes of the critical nucleus are larger, but the margin allowed for the growth is more limited (Gros et al., 2018). This means that the change in free energy between the critical nucleus and the stable crystallite is little, implying a less important superstraining effect at the melting process of the crystallite, usually leading to a smaller hysteresis in both crystalline degree and mechanical response. Furthermore, the interface energies were assumed to be constant, but they could depend on chain length, on temperature and on deformation. The fitted values given in Table 2 provide larger crystallite sizes than those experimentally measured but remain in the same order of magnitude. These sizes also depend on the choice of N^{topo} which we assumed to be given. The values of α allows to take into account the remarks given in a previous work (Gros et al., 2015) that the product $\gamma_e\gamma_l^2$ should be smaller by many order of magnitudes than that known in the literature (where γ_e and γ_l are of the same order of magnitude). Let us mention that the influence of the values of interface energies is extremely strong in our model.

Finally, the parameter that has not been studied in the above discussion is chain-length distribution. In the present model, longer chains crystallize first and the global threshold stretch ratio of crystallization (crystallization of the first population) is equal to $\widehat{\lambda_{c,i_{\max}}}\sqrt{\mathscr{N}^{\{0\}}}$ where $i_{\max}$ is the index of the population having the longest chains in the network: this relationship indicates that for a given $\widehat{\lambda_{c,i_{\max}}}$, crystallization starts later when $\mathscr{N}^{\{0\}}$ increases. In other words, crystallization starts the soonest when $\mathscr{N}^{\{0\}}$ is as small as possible and at concurrently when $i_{\max}$ is as large as possible. Besides, the chain-length distribution maximum mainly corresponds to the populations whose crystallization induces an important decrease in $\mathscr{N}^{\{s\}}$ (because of the large number of chains crystallizing), implying, in most cases, that crystallization is at its highest rate ($d\chi_c/d\lambda$) when these populations crystallize. That said, Fig. 8 shows that the

effect of chain-length distribution is limited on the macroscopic responses of nominal stress and crystalline degree.

5. Conclusion

In this paper, we derive a physically-based mechanical model for strain-induced crystallization of natural rubber. Its main features are the fact that it accounts for the chain-length distribution of the initial polymer network, that crystallization and melting are treated with a thermodynamical point of view, and after a classical integration to a 3D model, the establishment of a dedicated algorithm allowing most of the computation to be run independently of the applied deformation. The computed results qualitatively reproduce experiment crystalline degree evolution and mechanical response, and propose a new insight in the network evolution while crystallization occurs, promising further understanding of the physics of strain-induced crystallization in natural rubber.

A. Length of a 1D mesh

The end-to-end distance of an unstrained N_p-chain is not necessarily equal to that of a subchain of N_p segments belonging to an unstrained N-chain. Let us therefore consider a N-chain virtually divided into $\bar{\alpha}$ subchains of N_p segments ($p \in \{1\,;\,\dots\,;\,\bar{\alpha}\}$). Let $\overrightarrow{R_0} = l_0\vec{e}$ and let $\overrightarrow{R_p} = l_p\overrightarrow{r_p}$ be the end-to-end vectors of the chain and of the subchains respectively ($\vec{e}$ and $\overrightarrow{r_p}$ are unit vectors), and θ_p the angles $(\widehat{\overrightarrow{r_p}, \overrightarrow{e}})$. We thus have $\overrightarrow{R_0} = \sum_{p=1}^{\bar{\alpha}} \overrightarrow{R_p}$, and considering the projections on $\overrightarrow{R_0}$:

$$\overrightarrow{R_0}\cdot\overrightarrow{R_0} = \sum_{p=1}^{\bar{\alpha}}(\overrightarrow{R_p}\cdot\overrightarrow{R_0}) = \sum_{p=1}^{\bar{\alpha}}(l_p\overrightarrow{r_p}\cdot l_0\overrightarrow{e}) = l_0\sum_{p=1}^{\bar{\alpha}}(l_p\cos\theta_p)\,, \tag{41}$$

which means:

$$l_0 = \sum_{p=1}^{\bar{\alpha}}(l_p\cos\theta_p)\,. \tag{42}$$

Supposing that all the subchains have equal end-to-end distances, denoted l_0^{topo}, which means $\forall p,\ l_p = l_0^{\text{topo}}$ (*i.e.* $\forall p,\ N_p = N^{\text{topo}}$), the previous equation becomes:

$$l_0^{\text{topo}} = \left[\sum_{p=1}^{\bar{\alpha}}(\cos\theta_p)\right]^{-1} l_0\,. \tag{43}$$

Not knowing how to calculate the sum of the cosines, we simplify the problem by assuming that $\overrightarrow{R_0}$ and that $\overrightarrow{R_p}$ are collinear $\forall p$, which means:

$$l_0^{\text{topo}} = \bar{\alpha}^{-1}l_0 = \bar{\alpha}^{-1}\sqrt{N}b = \frac{N^{\text{topo}}}{\sqrt{N}}b\,. \tag{44}$$

where from its definition, $\bar{\alpha} = N/N^{\text{topo}}$, N^{topo} being the number of segments of a subchain. Assuming that chain deforms in an affine manner, we obtain:

$$l^{\text{topo}}(\lambda) = \lambda \frac{N^{\text{topo}}}{\sqrt{N}} b\,, \tag{45}$$

where λ is the stretch ratio applied to the whole chain.

B. Intermediate steps to obtain Eq. (12)

From derivations in Verron and Gros (2017) and from the resulting Eq. (4) in the present paper, the behavior of two chains deforming with an equal-force assumption can be averaged as:

$$\sqrt{N'_{\text{sub}}(N_{\text{sub1}}, N_{\text{sub2}})} = \frac{\phi_{\text{sub1}} N_{\text{sub1}} + \phi_{\text{sub2}} N_{\text{sub2}}}{\phi_{\text{sub1}} \sqrt{N_{\text{sub1}}} + \phi_{\text{sub2}} \sqrt{N_{\text{sub2}}}} \tag{46}$$

with $N_{\text{sub1}} + N_{\text{sub2}} = N - N_c$ and $\phi_1 = \phi_2$ since ϕ_i is their proportion in number of chain in the considered system. Defining $N_{\text{sub}} = N_{\text{sub1}} + N_{\text{sub2}}$, the equation simplifies to:

$$\sqrt{N'_{\text{sub}}(N_{\text{sub1}}, N_{\text{sub2}})} = \frac{N_{\text{sub1}} + N_{\text{sub2}}}{\sqrt{N_{\text{sub1}}} + \sqrt{N_{\text{sub2}}}} = \frac{N_{\text{sub}}}{\sqrt{N_{\text{sub1}}} + \sqrt{N_{\text{sub}} - N_{\text{sub1}}}}\,. \tag{47}$$

If all couples $(N_{\text{sub1}}, N_{\text{sub2}})$ verifying $N_{\text{sub1}} + N_{\text{sub2}} = N_{\text{sub}}$ are equiprobable, and supposing that all chains are undergoing equal-force assumption, we can make an average on all the possible $(N_{\text{sub1}}, N_{\text{sub2}})$ couples (and not a single one as for the previous equation) and obtain Eq. (12).

References

References

References

Albouy, P.-A., Guillier, G., Petermann, D., Vieyres, A., Sanseau, O., Sotta, P., 2012. A stroboscopic x-ray apparatus for the study of the kinetics of strain-induced crystallization in natural rubber. Polymer 53 (15), 3313–3324.
URL https://doi.org/10.1016/j.polymer.2012.05.042

Albouy, P.-A., Sotta, P., 2015. Strain-Induced Crystallization in Natural Rubber. Advances in polymer science. Springer Berlin Heidelberg, Berlin, Heidelberg, pp. 167–205.
URL http://dx.doi.org/10.1007/12_2015_328

Amnuaypornsri, S., Toki, S., Hsiao, B. S., Sakdapipanich, J., 2012. The effects of endlinking network and entanglement to stress-strain relation and strain-induced crystallization of un-vulcanized and vulcanized natural rubber. Polymer 53 (15), 3325–3330.
URL https://doi.org/10.1016/j.polymer.2012.05.020

Arruda, E. M., Boyce, M. C., 1993. A three-dimensional constitutive model for the large stretch behavior of rubber elastic materials. Journal of the Mechanics and Physics of Solids 41 (2), 389–412.
URL https://doi.org/10.1016/0022-5096(93)90013-6

Candau, N., Chazeau, L., Chenal, J.-M., Gauthier, C., Munch, E., 2015a. Compared abilities of filled and unfilled natural rubbers to crystallize in a large strain rate domain. Composites Science and Technology 108, 9–15.
URL http://dx.doi.org/10.1016/j.compscitech.2014.12.014

Candau, N., Chazeau, L., Chenal, J.-M., Gauthier, C., Munch, E., 2016. Complex dependence on the elastically active chains density of the strain induced crystallization of vulcanized natural rubbers, from low to high strain rate. Polymer 97, 158–166.
URL http://dx.doi.org/10.1016/j.polymer.2016.05.020

Candau, N., Laghmach, R., Chazeau, L., Chenal, J.-M., Gauthier, C., Biben, T., Munch, E., 2014. Strain-induced crystallization of natural rubber and cross-link densities heterogeneities. Macromolecules 47 (16), 5815–5824.
URL http://dx.doi.org/10.1021/ma5006843

Candau, N., Laghmach, R., Chazeau, L., Chenal, J.-M., Gauthier, C., Biben, T., Munch, E., 2015b. Temperature dependence of strain-induced crystallization in natural rubber: On the presence of different crystallite populations. Polymer 60, 115–124.
URL http://dx.doi.org/10.1016/j.polymer.2015.01.029

Candau, N., Laghrnach, R., Chazeau, L., Chenal, J.-M., Gauthier, C., Biben, T., Munch, E., 2015c. Influence of strain rate and temperature on the onset of strain induced crystallization in natural rubber. European Polymer Journal 64, 244–252.
URL http://dx.doi.org/10.1016/j.eurpolymj.2015.01.008

Flory, P. J., 1947. Thermodynamics of crystallization in high polymers. 1. crystallization induced by stretching. Journal of Chemical Physics 15 (6), 397–408.
URL http://dx.doi.org/10.1063/1.1746537

Flory, P. J., 1953. Principles of polymer chemistry. Baker lectures 1948. Cornell University Press.

Flory, P. J., Rehner, J. J., 1943. Statistical mechanics of cross-linked polymer networks. ii. swelling. The Journal of Chemical Physics 11, 521–526.
URL http://dx.doi.org/10.1063/1.1723792

Gros, A., Huneau, B., Verron, E., Tosaka, M., 2018. A physically-based model for strain-induced crystallization in natural rubber. part i: life cycle of a crystallite. Submitted to Journal of the Mechanics and Physics of Solids.

Gros, A., Tosaka, M., Huneau, B., Verron, E., Poompradub, S., Senoo, K., 2015. Dominating factor of strain-induced crystallization in natural rubber. Polymer 76, 230–236.
URL http://dx.doi.org/10.1016/j.polymer.2015.08.058

Guilié, J., Thien-Nga, L., Le Tallec, P., 2015. Micro-sphere model for strain-induced crystallisation and three-dimensional applications. Journal of the Mechanics and Physics of Solids 81, 58–74.
URL http://dx.doi.org/10.1016/j.jmps.2015.05.004

Holzapfel, G., 2003. Nonlinear solid mechanics: a continuum approach for engineering. Wiley.

Huneau, B., 2011. Strain-induced crystallization of natural rubber: a review of x-ray diffraction investigations. Rubber Chemistry and Technology 84 (3), 425–452.
URL http://dx.doi.org/10.5254/1.3601131

Ikeda, Y., Yasuda, Y., K, H., Tosaka, M., Kohjiya, S., 2008. Comparative study on strain-induced crystallization behaviour of peroxide cross-linked and sulfur cross-linked natural rubber. Macromolecules 41, 5876–5884.
URL http://dx.doi.org/10.1021/ma800144u

James, H. M., Guth, E., 1943. Theory of the elastic properties of rubber. The Journal of Chemical Physics 11 (10), 455–481.
URL http://dx.doi.org/10.1063/1.1723785

Khiêm, V., Itskov, M., 2016. Analytical network-averaging of the tube model:: Rubber elasticity. Journal of the Mechanics and Physics of Solids 95, 254 – 269.
URL https://doi.org/10.1016/j.jmps.2016.05.030

Khiêm, V., Itskov, M., 2018. Analytical network-averaging of the tube model: Strain-induced crystallization in natural rubber. Journal of the Mechanics and Physics of Solids 116, 350 – 369.
URL https://doi.org/10.1016/j.jmps.2018.04.003

Kroon, M., 2010. A constitutive model for strain-crystallising rubber-like materials. Mechanics of Materials 42 (9), 873–885.
URL http://dx.doi.org/10.1016/j.mechmat.2010.07.008

Laghmach, R., Candau, N., Chazeau, L., Munch, E., Biben, T., 2015. Phase field modelling of strain induced crystal growth in an elastic matrix. Journal of Chemical Physics 142 (24).
URL http://dx.doi.org/10.1063/1.4923226

Leitner, M., 1955. Young's modulus of crystalline, unstretched rubber. Transactions of the Faraday Society 51, 1015–1021.
URL http://dx.doi.org/10.1039/TF9555101015

Mark, J. E., 2006. Physical properties of polymers handbook, 2nd Edition. Springer.

Mark, J. E., 2009. The Polymer Data Handbook, 2nd Edition. Oxford University Press.

Miehe, C., Göktepe, S., Lulei, F., 2004. A micro-macro approach to rubber-like materials – part i: the non-affine micro-sphere model of rubber elasticity. Journal of the Mechanics and Physics of Solids 52 (11), 2617–2660.
URL http://dx.doi.org/10.1016/j.jmps.2004.03.011

Mistry, S. J., Govindjee, S., 2014. A micro-mechanically based continuum model for strain-induced crystallization in natural rubber. International Journal of Solids and Structures 51 (2), 530–539.
URL http://dx.doi.org/10.1016/j.ijsolstr.2013.10.027

Nateghi, A., Dal, H., Keip, M.-A., Miehe, C., 2018. An affine microsphere approach to modeling strain-induced crystallization in rubbery polymers. Continuum Mechanics and Thermodynamics 30 (3), 485–507.
URL https://doi.org/10.1007/s00161-017-0612-8

Plagge, J., Klüppel, M., 2018. A theory relating crystal size, mechanical response, and degree of crystallization in strained natural rubber. Macromolecules 51 (10), 3711–3721.
URL https://doi.org/10.1021/acs.macromol.8b00177

Rastak, R., Linder, C., 2018. A non-affine micro-macro approach to strain-crystallizing rubber-like materials. Journal of the Mechanics and Physics of Solids 111, 67–99.
URL https://doi.org/10.1016/j.jmps.2017.10.007

Sloan, I. H., Womersley, R. S., 2004. Extremal systems of points and numerical integration on the sphere. Advances in Computational Mathematics 21 (1), 107–125.
URL http://dx.doi.org/10.1023/B:ACOM.0000016428.25905.da

Smith, W. H., Hanna, N. P., 1941. Comparison between the observed density of crystalline rubber and the density calculated from x-ray data. Journal of Research of the National Bureau of Standards 27 (3), 229–236.
URL https://doi.org/10.5254/1.3546606

Steenbakkers, R. J. A., Tzoumanekas, C., Li, Y., Liu, W. K., Kröger, M., Schieber, J. D., 2014. Primitive-path statistics of entangled polymers: mapping multi-chain simulations onto single-chain mean-field models. New Journal of Physics 16, 015027.
URL http://dx.doi.org/10.1088/1367-2630/16/1/015027

Toki, S., 2014. Chemistry, manufacture and applications of natural rubber. Woodhead Publishing, Ch. The effect of strain-induced crystallization (SIC) on the physical properties of natural rubber (NR).

Toki, S., Sics, I., Ran, S., Liu, L., Hsiao, B. S., Murakami, S., Tosaka, M., Kohjiya, S., Poompradub, S., Ikeda, Y., Tsou, A. H., 2004. Strain-induced molecular orientation and crystallization in natural and synthetic rubbers under uniaxial deformation by *in-situ* synchrotron x-ray study. Rubber Chemistry and Technology 77 (2), 317–335.
URL http://dx.doi.org/10.5254/1.3547826

Toki, S., Sics, I., Ran, S. F., Liu, L. Z., Hsiao, B. S., SEP 2003. Molecular orientation and structural development in vulcanized polyisoprene rubbers during uniaxial deformation by *in situ* synchrotron X-ray diffraction. Polymer 44 (19), 6003–6011.

Tosaka, M., 2007. Strain-induced crystallization of crosslinked natural rubber as revealed by x-ray diffraction using synchrotron radiation. Polymer Journal 39, 1207–1220.
URL http://dx.doi.org/10.1295/plymj.PJ2007059

Tosaka, M., Senoo, K., Sato, K., Noda, M., Ohta, N., 2012. Detection of fast and slow crystallization processes in instantaneously-strained samples of cis-1,4-polyisoprene. Polymer 53 (3), 864–872.
URL http://dx.doi.org/10.1016/j.polymer.2011.12.035

Trabelsi, S., Albouy, P.-A., Rault, J., 2003. Crystallization and melting processes in vulcanized stretched natural rubber. Macromolecules 36 (20), 7624–7639.
URL http://dx.doi.org/10.1021/ma030224c

Treloar, L. R. G., 1954. The photoelastic properties of short-chain molecular networks. Transactions of the Faraday Society 50, 881–896.
URL http://dx.doi.org/10.1039/TF9545000881

Treloar, L. R. G., 1975. The physics of rubber elasticity. Monographs on the physics and chemistry of materials. Oxford University Press.

Treloar, L. R. G., Riding, G., 1979. A non-gaussian theory for rubber in biaxial strain. i. mechanical properties. Proceedings of the Royal Society of London A: Mathematical, Physical and Engineering Sciences 369 (1737), 261–280.
URL http://dx.doi.org/10.1098/rspa.1979.0163

Verron, E., 2015. Questioning numerical integration methods for microsphere (and microplane) constitutive equations. Mechanics of Materials 89, 216–228.
URL http://dx.doi.org/10.1016/j.mechmat.2015.06.013

Verron, E., Gros, A., 2017. An equal-force theory for network models of soft materials with arbitrary molecular distribution. Journal of the Mechanics and Physics of Solids 106, 176–190.
URL https://doi.org/10.1016/j.jmps.2017.05.018

Wang, M. C., Guth, E., 1952. Statistical theory of networks of non-gaussian flexible chains. The Journal of Chemical Physics 20 (7), 1144–1157. URL http://dx.doi.org/10.1063/1.1700682

Wood, L. A., Bekkedahl, N., 1946. Crystallization of unvulcanized rubber at different temperatures. Rubber Chemistry and Technology 19 (4), 1145–1162. URL http://dx.doi.org/10.5254/1.3543253

Wu, P. D., van der Giessen, E., 1993. On improved network models for rubber elasticity and their applications to orientation hardening in glassy polymers. Journal of the Mechanics and Physics of Solids 41 (3), 427–456. URL http://dx.doi.org/10.1016/0022-5096(93)90043-F